J. Condensed Matter Nucl. Sci. 34 (2021) 32–58

Research Article

Interpreting CR-39 Detectors used in Pd/D Co-deposition: Nuclear Generated Tracks or Artifacts?

P.A. Mosier-Boss* and L.P. Forsley

GEC, 5101B Backlick Rd., Annandale, VA 22003, USA

Abstract

In this communication we summarize relevant results obtained for CR−39 detectors used in Pd/D co-deposition experiments. These results include evidence of neutrons, notably 14.1 MeV neutrons, and control experiments to rule out chemical/mechanical damage as the source of the pitting. The SRI replication is discussed. The CR-39 detectors used in this replication underwent exhaustive analysis by noted CR-39 experts from NASA and Russian Academy of Sciences. We also address alternative explanations offered by other researchers as to the source of the pitting in CR-39 detectors used in Pd/D co-deposition. These include deuteroxide/O_2 attack, shockwaves resulting from D_2/O_2 recombination, and corona discharge. We also explored why the pits are primarily circular in shape and why the emission of Pd K shell X-rays is not observed.
 ISSN 2227-3123

Keywords: Controls, CR-39, Energetic particles, Pd/D co-deposition

1. Introduction

CR-39 is a highly cross-linked, thermoset polymer that is inexpensive, chemically resistant, and exhibits both high abrasion and impact resistance. Its most common use is in optics, in particular the lenses of eyeglasses. However, CR-39 is also widely used as a solid state nuclear track detector (SSNTD) in the inertial-confinement-fusion (ICF) field to detect the energetic charged particles and neutrons created upon laser compression of the DT fuel capsule [1]. One primary reason for its use is that CR-39 is not affected by the electromagnetic pulse (EMP) that disables electronic detectors in an ICF experiment. Besides cost and ruggedness, other properties that make CR-39 attractive for use in the ICF field are its integrating capability and degree of charge and energy discrimination [2]. These same attributes make CR-39 ideal for use in the detection of energetic particles in the Pd/D system. Such energetic particles have been detected, using CR-39 detectors, in both gas loading [3] and electrolytic [4–8] loading experiments. In the gas loading experiments [3], bulk Pd foils were in direct contact with the detectors. In some electrolytic loading experiments [6,8], bulk Pd foils or films were in contact with CR-39 detectors during electrolysis. For other experiments, electrolytically

*Corresponding author. E-mail: pboss@san.rr.com.

 ISSN 2227-3123

loaded Pd/D foils were removed from solution and placed in contact with CR-39 to detect energetic particles during exothermic desorption of deuterium out of the foils [4,5,7].

In 2006, we began conducting experiments using CR-39 detectors during Pd/D co-deposition. In Pd/D co-deposition, Pd is electroplated, in the presence of evolving deuterium gas, onto a non-hydriding electrode surface. In these experiments, the CR-39 detector is placed in close proximity to the cathode since charged particles do not travel far through water [9]. Linear energy transfer (LET) curves indicate that a 10μm thick film of water can stop a 1.8 MeV alpha particle. Tracks in CR-39, on both the front and back surfaces, have been obtained in the Pd/D co-deposition experiments [10]. The optical properties of the Pd/D co-deposition generated tracks were the same as those observed for nuclear generated tracks [9,10]. Specifically, when the microscope optics were focused on the surface of the detector, the tracks are dark in color and either circular or elliptical in shape. When the microscope optics were focused inside the tracks, bright points of light are observed for both the Pd/D co-deposition and the nuclear-generated tracks. These bright points are due to the rounded bottom of the track acting like a lens when the detector is backlit. The Pd/D co-deposition and nuclear generated tracks both exhibit high optical contrast. The optical contrast, shape, and bright spot in the center of the track are used to differentiate real particle tracks from false events which tend to be lighter in appearance and irregular in shape. A series of control experiments showed that the tracks were not due to radioactive contamination of the cell components. Experiments were conducted that indicated, to us, that the pitting was not due to mechanical or chemical damage. Despite these efforts, it has been suggested, over the years by several researchers, that the pitting observed in the detectors after Pd/D co-deposition are not due to nuclear events occurring within the Pd lattice. Rather they are due to shock waves resulting from D_2/O_2 recombination, corona discharge, and/or mechanical/chemical damage. The question was raised that, if all these charged particles were being created, why were no X-ray emissions from Pd observed? In this communication, we address these, as well as other, issues brought up by researchers on the interpretation of the CR-39 results obtained as a result of Pd/D co-deposition.

2. Summary of Relevant Pd/D Co-deposition Results

2.1. Pd/D Co-deposition on Ni screen

Our early experiments used Ni screen as the cathode [9]. The Ni screen was placed in contact with the CR-39 detector. Both the detector and the Ni screen cathode were immersed in the $PdCl_2$–LiCl–D_2O solution and Pd was then plated out in the presence of evolving deuterium gas. Upon completion of the experiment, the cell was taken apart and the CR-39 detector was etched in a 6.5 M NaOH solution at 65–72°C for 6–7 h. Figure 1a is a photograph taken of the detector. The photograph shows an impression of the Ni screen. A photomicrograph of the detector obtained at 20× magnification, after etching, is shown in Fig. 1b. No tracks were observed and the area around the hollows appear to be swollen. A few months later another photomicrograph was obtained at 20× magnification, Fig. 1c. This image shows that the swelling has increased. No such swelling was observed in detectors that showed either track damage or chemical damage caused by reaction with either hydroxide or oxygen. Swelling and an impression of a screen have been observed for a detector that had been wrapped with a metal screen and exposed to a ^{137}Cs γ-ray source, which has a characteristic 662 keV peak. This suggests that the damage shown in Fig. 1a–c was due to exposure to either X- or γ-rays.

There have been previous reports of X-ray emission by Pd/D substrates as measured using photographic film [11,12], HPGe γ-ray and Li-doped Si X-ray detectors [13,14], and CaF_2 thermoluminescence dosimeters [3]. Figure 1d shows fogging of photographic film after a Pd/D co-deposition experiment was conducted on the Ag disk of a piezoelectric crystal [9]. Not only can the circular shape of the cathode be seen, but the emission of X-rays is not homogeneous. The swelling observed in the detector results from scissioning of the molecular chains by irradiation with γ- and X-rays [15,16]. The bond breaking gives rise to free radicals, water molecules, and gaseous products [15].

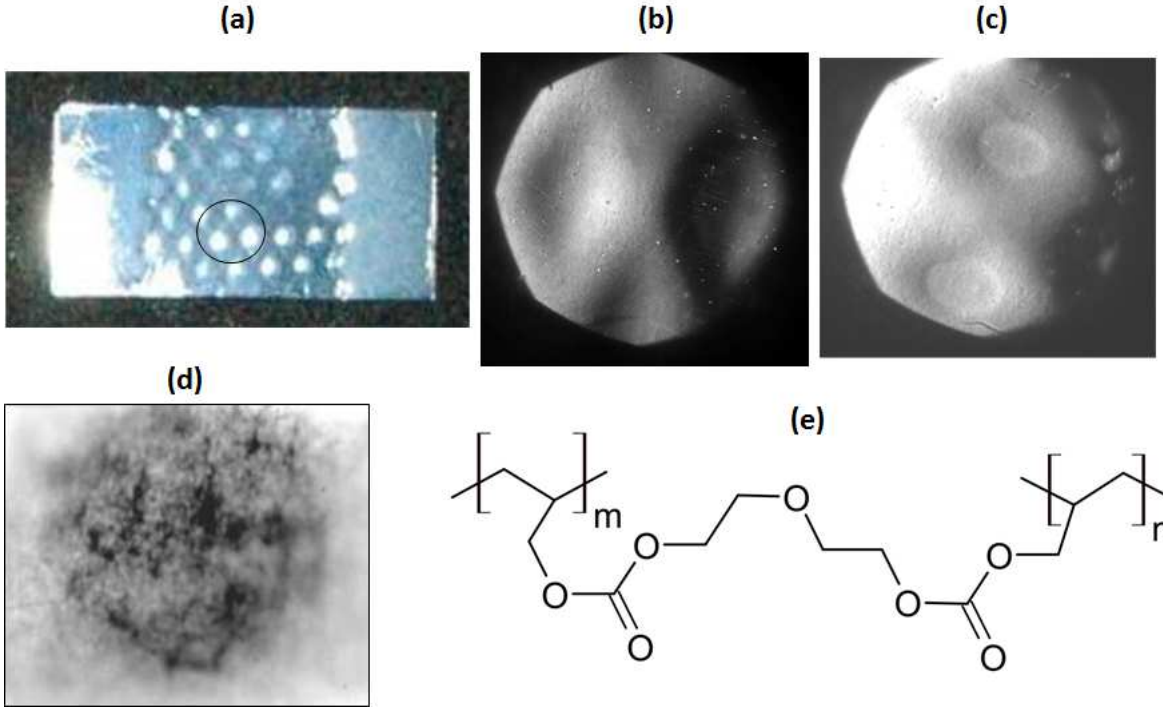

Figure 1. Phtograph of a CR-39 detector that was used in a Pd/D co-deposition experiment conducted on a Ni screen cathode in the absence of an external magnetic/electric field. (b) and (c) Photomicrographs of the circled area shown in (a) obtained at a magnification of 20X where (b) was taken right after etching the detector and (c) was taken several months later. (d) Fogging of photographic film after three day exposure to Pd deposited in a Ag disk cathode (a thin sheet of Mylar separated the film from the cathode). (e) Structure of CR-39.

In the case of CR-39, whose structure is shown in Fig. 1e, bond breaking, caused by irradiating the plastic with γ- or X-rays, produces CO_2. The trapped gas causes swelling of the resin [17].

Significantly different results were obtained when Pd/D co-deposition on a Ni screen cathode was done in the presence of either an external electric or magnetic field [9]. In these experiments, the external electric/magnetic field was applied after the Pd had plated out on the Ni screen. The electric field typically used was 6000 V DC with a $\sim$6% AC component ripple that allowed for magnetic coupling into the cathode. Photomicrographs of the detector used in a magnetic field experiment are shown in Fig. 2. Similar results were obtained when an external electric field was applied. Figure 2a shows a photomicrograph taken at 20X magnification. No swelling of the detector is observed. Damage to the CR-39 detector is observed where the Pd deposit was in contact with the surface of the plastic. The jagged outlines of the Ni screen can be seen. Figure 2b shows part of this outline at higher magnification (200X). A large number of circular pits is observed. As shown in Fig. 2a, the density of pits is greater where the Pd deposit is thickest. This is especially true inside the eyelets of the Ni screen. Figure 2c shows the pits in an eyelet at a magnification of 200X. In 2006, this image was shown to Samuel Roberts, a senior laboratory engineer at the University of Rochester's Laboratory for Laser Energetics (LLE) involved in the developing of CR-39 analytics and is an expert in the interpretation of CR-39 [1,2,18,19]. Based upon the energy deposition curve of CR-39, he estimated that the tracks were caused by either very low energy alphas (<500 keV) or very high energy protons (>7 or 8 MeV).

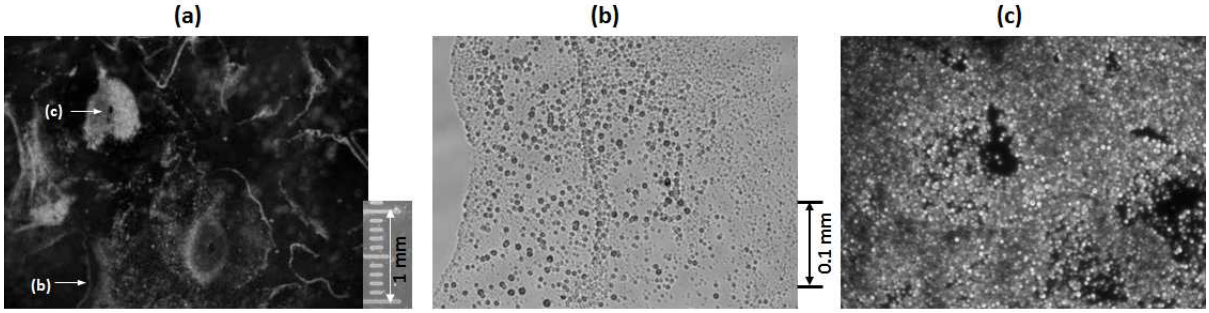

Figure 2. Photomicrographs of a CR-39 detector that was used in a Pd/D co-deposition experiment conducted on a Ni screen cathode in the presence of an external magnetic field. Magnifications are (a) 20× and (b), (c) 200×. The areas obtained at higher magnification in (a) are indicated.

Additional experiments were done using higher Z substrates (Ag, Pt, and Au wires) as cathodes for Pd/D co-deposition [9]. Figure 3a and b shows photomicrographs obtained for a CR-39 detector used in a Pd/D co-deposition experiment done of a Ag wire cathode in the absence of either an external magnetic/electric field. In contrast with the Ni screen experiments, the higher Z cathodic substrates do not require an external electric or magnetic field to generate pits in the CR-39 detector. Regardless of the high Z cathode substrate used for Pd/D co-deposition, cloudy areas were

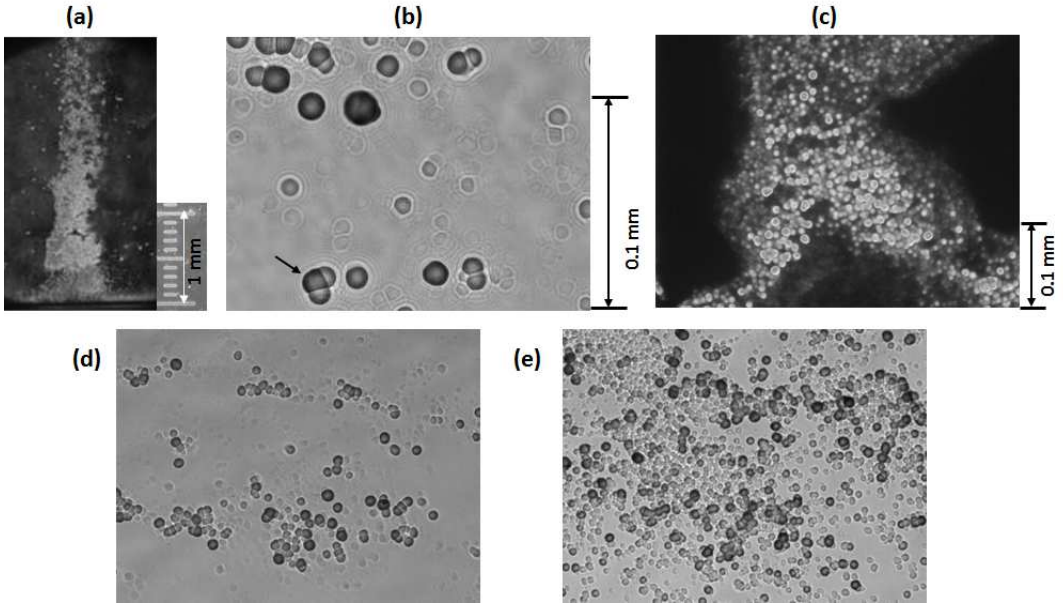

Figure 3. (a and b) Photomicrographs of a CR-39 detector that was used in a Pd/D co-deposition experiment conducted on a Ag wire cathode in the absence of an external electric/magnetic field. Magnifications are (a) 20× and (b) 500× (arrow indicates a triple track). (c) Photomicrograph of a CR-39 detector that was used in a Pd/D co-deposition experiment conducted on a Ni/Au screen cathode in the absence of an external magnetic field. Magnification is 200×. (d) and (e) Photomicrographs of CR-39 detectors used in Ag/Pd/D co-deposition in H_2O and D_2O, respectively. Magnification is 200×. The H_2O and D_2O experiments were done in an external electric and magnetic field, respectively.

observed where the Pd-coated wires were in contact with the detector, Fig. 3a. Higher magnification shows that within these cloudy areas there are copious numbers of pits. The density of pits decreases the further away one gets from where the Pd deposit was in contact with the detector. In areas where the density of pits is low, Fig. 3b, it can be seen that there are both large and small pits as well as a triple pit, indicated by an arrow. The significance of triple pits, or tracks, will be discussed *vide infra*. The difference between Ni screen and higher Z metal wires could be attributed to either the electrode substrate or to the current density (individual wires will exhibit a higher current density than a screen). To rule out current density, an experiment was done where Au was electroplated on the Ni screen. Then Pd/D co-deposition was done on this Ni/Au cathode that was in contact with a CR-39 detector. Pits were obtained as shown in Fig. 3c. This implies that the difference is due to some metallurgical property of the cathode materials. Given that external magnetic/electric fields induce track formation in Ni screen, magnetic properties of metals may play a role. Of the cathode materials used in these studies, Ni is ferromagnetic, Ag and Au are diamagnetic, and Pt and Pd are paramagnetic. Consequently, Ni would be more strongly influenced by a magnetic field than the other metals. Recently DeChairo et al. [20] ran spin-polarized density functional theory (DFT) calculations showing that strained layer ferromagnetism played a role in inducing low energy nuclear reactions (LENR). This correlation needs to be investigated further as it may provide a way to control and increase LENR reproducibility.

2.2. Summary of control experiments

A series of control experiments were done that showed that the pits in the CR-39 detectors were not due to radioactive contamination of the cell components nor were they due to mechanical or chemical damage [9]. The experiments done are summarized in Table 1. The time duration of these control experiments were the same as that used in the Pd/D co-deposition experiments. No pitting was observed when cathode substrates and $PdCl_2$ powder were placed in contact with CR-39 or when a CR-39 detector was immersed in the $PdCl_2$–LiCl–D_2O plating solution. This indicated that the pitting was not due to radioactive contamination. To verify that pitting in CR-39 detector was not caused by the evolution of D_2 bubbles or the reducing conditions of the cathode, electrolysis experiments were conducted by wrapping either a Ni or a Cu screen around a CR-39 detector. This cathode/CR-39 composite was immersed in a solution of LiCl in D_2O and electrolysis was done by applying a cathodic current of 50 mA. Vigorous gas evolution was observed on the cathode, more so than was observed for Pd/D co-deposition. After etching, no pits were observed where the Ni/Cu screen had been in contact with the detector nor was there an impression of the Ni/Cu screen on the surface as had been observed for Pd/D co-deposition done on Ni screen in the absence of an external magnetic/electric field. These results indicate that the pits are not due to the impingement of D_2 gas bubbles on the surface of the CR-39 or from reactions between D_2 and CR-39. Because the D_2 and O_2 gases were free to mix in these experiments, the pitting is not due to reactions between O_2 and CR-39.

A co-deposition experiment was done on a Ag wire in H_2O in the presence of an external electric field [9]. Visual examination of the detector, after etching, showed sparse patches of cloudy areas along the length of the Ag/Pd wire. Figure 3d shows one such patch at a magnification of 200×. Although tracks are observed in this patch, the track density is several orders of magnitude less than was observed for D_2O co-deposition in an external magnetic field, Fig. 3e. These results are also consistent with the reports of energetic particles for light water electrolysis experiments using thin Pd foils [6].

The most notable of all these control experiments was the electroplating of Cu or Ni instead of Pd. In the Pd, Cu, and Ni electroplating experiments, a metal is plating out in the presence of evolving D_2 gas on the cathode. At the anode, O_2 and Cl_2 gas evolution occurs. The Pd, Cu, and Ni deposits exhibit similar morphologies. The only significant difference between these systems is that Pd absorbs deuterium at ambient temperatures and pressures, but Cu and Ni do not, as shown when the current is turned off. The Pd deposit formed from Pd co-deposition vigorously outgases for several minutes when the current ceases. No such outgassing was observed for the Cu and Ni deposits.

Table 1. Summary of control experiments done.

Experiment[a]	Results of CR-39[b]
Pd, Ag, Au, and Pt wires in contact with CR-39 immersed in H_2O, no electrolysis	No pits observed, no impression of the wires
$PdCl_2$ powder placed on top of CR-39, no electrolysis	No pits observed
CR-39 detector placed in $PdCl_2$-LiCl-D_2O plating solution, no electrolysis	No pits observed
Cu screen on CR-39 immersed in LiCl-D_2O solution, electrolysis at $I = -50$ mA	No pits observed, no impression of the screen
Ni screen on CR-39 immersed in LiCl-D_2O solution, electrolysis at $I = -50$ mA	No pits observed, no impression of the screen
Ag wire on CR-39 immersed in $CuCl_2$-LiCl-D_2O plating solution, same electrolysis profile used in Pd/D co-deposition	No pits observed. Observe a shallow groove in the detector where the wire and metal deposit were in contact with the detector. No swelling around this groove was observed with time
Ag wire on CR-39 immersed in $NiCl_2$–LiCl–D_2O plating solution, same electrolysis profile used in Pd/D co-deposition	No pits observed. Observe a shallow groove in the detector where the wire and metal deposit were in contact with the detector. No swelling around this groove was observed with time
Ag wire on CR-39 immersed in $PdCl_2$–LiCl–H_2O plating solution, same electrolysis profile used in Pd/D co-deposition, experiment done in an external electric field	See hollow where Pd that was deposited on the wire was in contact with CR-39 detector. See bursts of pits. Density of pits far less than observed for Pd/D co-deposition

[a] Each experiment was conducted over a 2–3 weeks period.

[b] In this context, 'no pits' is used to indicate that the number of pits observed was not in excess to what was commonly observed as a result of background emissions. Also what pits were observed were not directly associated with the placement of the cathode substrate on the detector.

At room temperature, Ni powder absorbs about 0.45 wt.% at 4.5 MPa (44.4 atm) H_2 pressure [21]. While tracks were observed for the Pd/D electroplating, none were observed for either the Cu/D or Ni/D electroplating system. These control experiments indicate that the tracks observed in the Pd/D co-deposition experiments are not due to chemical attack of the surface of the CR-39 detector by D_2, O_2, or Cl_2 gases; or due to the metal dendrites piercing into the CR-39. A shallow groove was observed in the CR-39 detectors used in the Cu/D and Ni/D electroplating experiments that corresponded to the placement of the wire and metal deposit on the detector. Microscopic examination of the groove showed that there were no pits. Likewise no swelling of this groove was observed to occur with time so the damage is not due to γ-/X-ray damage. During electrolysis of D_2O/H_2O, OD^-/OH^- ions are formed at the cathode. These electrochemically produced ions will etch the detector and are responsible for the formation of the shallow groove. This also indicates that chemical damage will not cause swelling of the detector.

2.3. Evidence of neutrons: tracks on the backside and triple tracks

In addition to tracks on the front surface of the CR-39 detectors where the cathode and deposit are in contact with the detector, tracks have also been observed on the backside of the 1 mm thick detectors, Fig. 4a [10]. From LET curves, the only energetic particles that can go through a 1 mm thick CR-39 detector are $\geq$ 43 MeV alphas, $\geq$ 10 MeV protons, or neutrons. Unlike charged particles, neutrons do not directly cause an ionization trail in the plastic. However, neutrons can scatter elastically anywhere inside the detector, producing recoil protons, carbons, or oxygen nuclei in the forward direction [1]. These elastic scatterings cause tracks on the backside of a CR-39 detector. Figure 4b shows a photomicrograph of tracks in a CR-39 detector resulting from exposure to a ^{238}PuO, broad-spectrum neutron source. In both photomicrographs shown in Fig. 4, it can be seen that the tracks are primarily circular in shape. However, some tracks are circular with a small tail. These are recoil protons that have interacted with the CR-39 at an angle less

than 90º. Small tracks are also observed in these photomicrographs. Since neutron interactions can occur anywhere throughout the CR-39 detector, these smaller tracks are attributed to neutron-plastic interactions that occurred deeper inside the CR-39 detector.

Besides scattering, energetic neutrons can also react with a carbon in the CR-39 to create a metastable ^{13}C atom, which then shatters into three alpha particles [1]. The residuals of this reaction can be viewed in the CR-39 detector as a three-prong star where each prong represents each charged particle reaction product [22]. The threshold energy of the neutron required to shatter a carbon atom to form a three-prong star is 9.6 MeV [23]. Triple tracks have been observed in CR-39 detectors used in Pd/D co-deposition experiments. An example of such a triple track is shown in Fig. 5a [24]. This triple track is observed in an area of low track density. It is surrounded by a number of solitary tracks. Given that the density of tracks in this region is low, it is unlikely that this triple track is due to overlapping tracks. The track was examined at higher magnification. Figure 5b shows two images taken at different focal lengths. The left image was taken with the optics focused on the surface of the detector. The right image is an overlay of two images taken at two different focusing depths (surface and the bottom of the pits). The latter image shows three individual lobes breaking away from a center point. Figure 5c shows images of triple tracks similar to one shown in Fig. 5b that were generated by exposing CR-39 detectors to a DT fusion neutron source. The nominal energy of the neutrons the created these tracks was 14.1 MeV.

Figure 6 shows side by side comparisons of triple tracks in CR-39 detectors produced as a result of Pd/D co-deposition experiments that are similar to those created upon exposure to a DT neutron source [25]. No triple tracks were observed in CR-39 detectors used in control experiments. As discussed *vide supra*, the left image of each set was taken with the optics focused on the surface and the right image is an overlay of two images taken at different focusing depths (surface and the bottom of the pits). In both the Pd/D co-deposition and DT neutron images, the images taken at the surface look like overlapping tracks. However, by focusing the optics inside the triple tracks (right images of each set), it can be seen that the individual lobes making up the triple tracks are emanating from a center point. According to Roussetski [5], a CR-39 expert from the P.N. Lebedev Physical Institute of the Russian Academy of Sciences, "the presence of three α-particle tracks outgoing from a single point allows us to separate these (carbon break-up) reactions from other neutron interactions with CR-39 detectors." As shown in Fig 6, the triple tracks do not exhibit the same shape. The lobes comprising each triple track clearly do not have the same size. This is attributed to the fact that the n + ^{12}C reaction can proceed to the four-body final state through one or more of the following reaction mechanisms [22]:

$$n + {}^{12}\mathrm{C} \rightarrow n' + \alpha + ({}^{8}\mathrm{Be} \rightarrow 2\alpha), \tag{1}$$

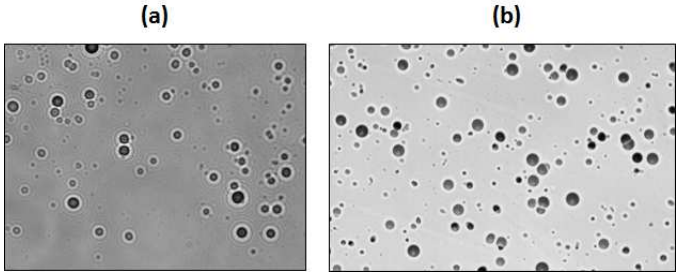

Figure 4. Photomicrographs, obtained at 200× magnification, of (a) the backside of a CR-39 detector used in a Pd/D co-deposition experiment done on a Ag wire and in the presence of an external magnetic field and (b) CR-39 exposed to a ^{238}PuO neutron source.

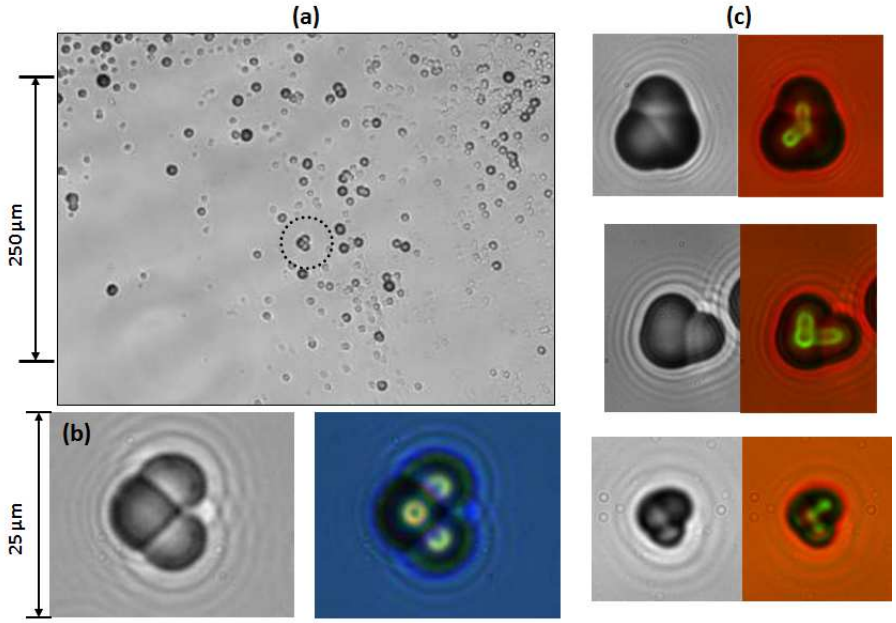

Figure 5. Photomicrographs of CR-39 detectors used in a Pd/D co-deposition experiment (a and b) and a CR-39 detector exposed to a DT neutron source (c). (a) An image of a triple track (circled) among solitary tracks obtained at 200× magnification. (b) Image of the triple track in (a) at 1000× magnification. (c) Images of DT neutron generated triple tracks similar to the one shown in (b) taken at 1000× magnification. In (b) and (c), the left image was obtained with the optics focused on the surface of the detector. The right image is an overlay of two images taken at two focal lengths (surface and bottom of the pits).

$$n + {}^{12}\mathrm{C} \rightarrow \alpha + ({}^{9}\mathrm{Be} \rightarrow n' + ({}^{8}\mathrm{Be} \rightarrow 2\alpha)), \tag{2a}$$

$$n + {}^{12}\mathrm{C} \rightarrow \alpha + ({}^{9}\mathrm{Be} \rightarrow \alpha + ({}^{5}\mathrm{He} \rightarrow n' + \alpha)), \tag{2b}$$

$$n + {}^{12}\mathrm{C} \rightarrow ({}^{8}\mathrm{Be} \rightarrow 2\alpha) + ({}^{5}\mathrm{He} \rightarrow n' + \alpha), \tag{3}$$

$$n + {}^{12}\mathrm{C} \rightarrow n' + \alpha + \alpha + \alpha \tag{4}$$

as well as the recoil energy exceeding the binding energy being unevenly distributed amongst the reaction products. Processes (1)–(3) are sequential decays going through different intermediate excited states and process (4) is a simultaneous four-body break-up. When shown photomicrographs of the Pd/D co-deposition generated triple tracks, Johan Frenje [26], senior research scientist of MIT's Plasma Science and Fusion Center and DoE's expert on interpreting CR-39 tracks, said, "I must say that the data and their analysis seem to suggest that energetic neutrons have been produced."

2.4. The SRI replication during the Galileo project

On Nov. 10, 2006, the New Energy Institute headed by Steve Krivit initiated the Galileo Project. The goal of the project was to have other scientists 'skilled in the art' replicate the Pd/D co-deposition results obtained using CR-39. One of the groups involved in the replication were Fran Tanzella et al. from SRI [27,28]. The SRI group did

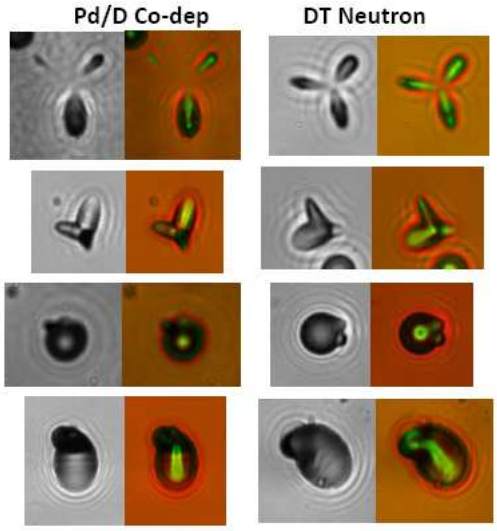

Figure 6. Photomicrographs comparing Pd/D co-deposition generated triple tracks in CR-39 with those produced by a DT neutron generator. For both sets of photomicrographs, the left image was obtained with the optics focused on the surface of the detector. The right image is an overlay of two images taken at two focal lengths (surface and bottom of the pits). Images were taken at 1000× magnification.

experiments with the CR-39 detector immersed inside the cell with the cathode in contact with the CR-39 detector as well as experiments with the CR-39 detector outside the cell. In the latter experiment, a 6 μm thick Mylar film separated the detector from the cathode. For both sets of experiments, Pd/D co-deposition was done on an Ag wire cathode in the presence of an external magnetic field throughout the course of the experiment. This deviated from the original protocol [9] which called for application of the external magnetic field after the Pd had plated out. In the immersion experiments, a 60 μm polyethylene film separated the cathode from the CR-39 detectors. Fukuvi-brand CR-39 detectors come with this film which protects the detectors from mechanical damage, such as scratching, and blocks $\leq$7 MeV alphas and $\leq$1.8 MeV protons. By blocking $\leq$7 MeV alphas, the film essentially prevents the detectors from registering background radiation due to radon and dust particles containing uranium/thorium isotopes. The presence of this film deviated from the original experimental protocol [9] which instructed removal of the protective film from the detector prior to use in the Pd/D co-deposition experiments. In the 'outside the cell' experiment, this polyethylene film was removed from the detector before it was pressed against the Mylar film and was held in place by magnets [28].

Figures 7a shows a photomicrograph obtained for a CR-39 detector used in Pd/D co-deposition experiments without the 60 μm thick polyethylene film between the detector and the cathode [27]. A high density of overlapping tracks is observed. When experiments were done with the 60 μm thick polyethylene film between the detector and the cathode, a significant decrease in the number of tracks was observed, Fig. 7b. Detectors from both the immersion experiments and the 'outside the cell' experiment were subjected to sequential etching analysis [28]. Figure 7c shows the size distribution of tracks obtained after etching detectors used in the immersion experiments for 21 h. This size distribution was obtained by taking the difference of the nuclear track distribution on the front side of the detector and that from the neutron induced proton recoil track distribution from its backside normalized to the highest count (front –1.4 $\times$ back side). Using calibration curves for protons and alphas measured as a function of etching time, the particles responsible for the tracks were identified and are indicated in Fig. 7c. Sequential etching of the detector

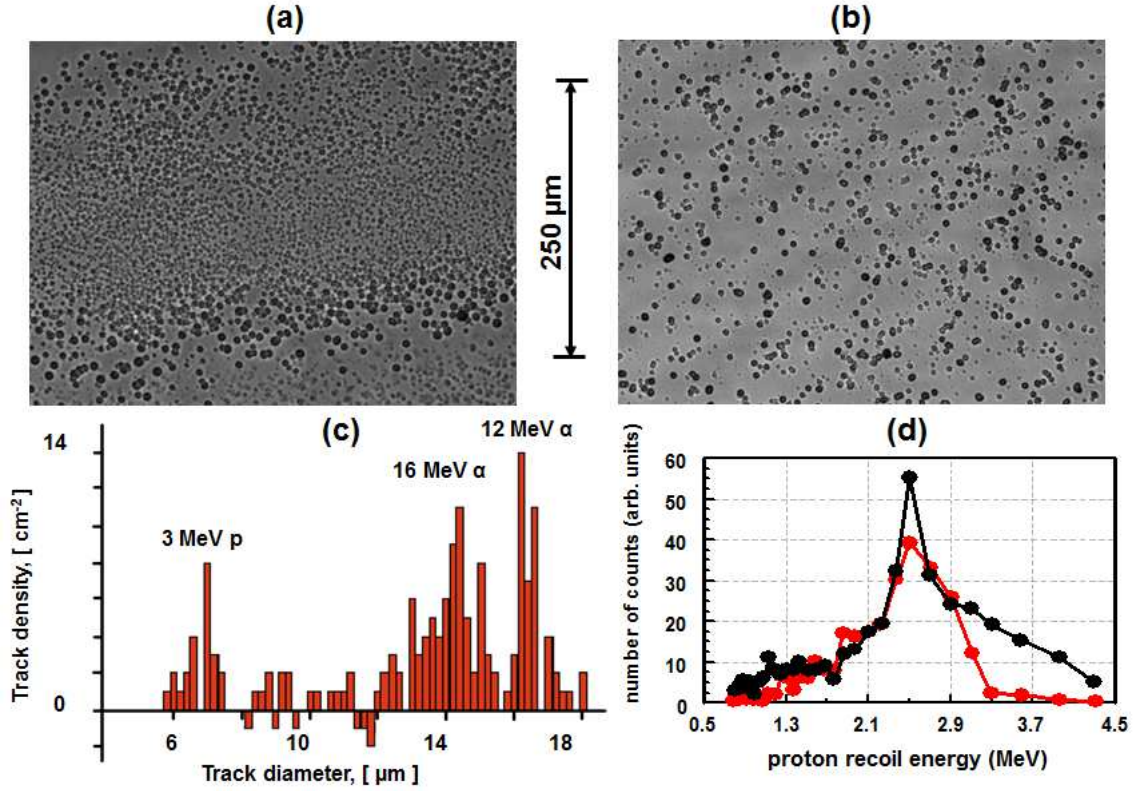

Figure 7. Photomicrographs obtained at 200× magnification for CR-39 detectors used in an immersion Pd/D co-deposition (a) without and (b) with 60 μm polyethylene covers between the cathode and the detector. The time duration of both experiments was the same. (c) Measured size distribution obtained after a 21 h etch of the CR-39 detector used in the immersion experiment. Energetic particles responsible for the tracks are indicated. (d) Reconstruction of the protons recoil spectra from both the non-immersion D_2O run and ^{252}Cf exposure.

used in the 'outside the cell' D_2O experiment, showed tracks due to proton recoils from fast neutrons. No such tracks were observed in background detectors or detectors used in light water experiments. Figure 7d shows proton recoil spectra reconstructed from sequential etching of CR-39 detectors exposed to a ^{252}Cf neutron source and the detector used in the 'outside the cell' D_2O experiment. For the non-immersed D_2O experiment, the energy of the neutrons was determined to be 2.5 MeV and the neutron count rate was estimated to be 0.6±0.1 count/s.

The detectors used in the SRI immersion experiments were scanned using an automated scanner that obtained quantitative information on the pits [27]. We had also conducted an 'outside the cell' experiment similar to the one done by SRI [29]. Like the SRI experiment, Pd/D co-deposition was done in the presence of an external magnetic field and a 6 μm thick Mylar film separated the Au and Pt cathodes from the detector that was placed outside the cell. Upon completion of the experiment, this CR-39 detector was also scanned. The proprietary software used by the scanner makes 15 characteristic measurements of each feature in the detector. Measurements include track length and diameter, optical density (average image contrast), and image symmetry. Based upon the measured properties of a given feature, the software algorithms determine whether or not the feature is a track due to an energetic particle. Figure 8a and b shows the size distributions of the tracks measured for the immersion and 'outside the cell' detectors,

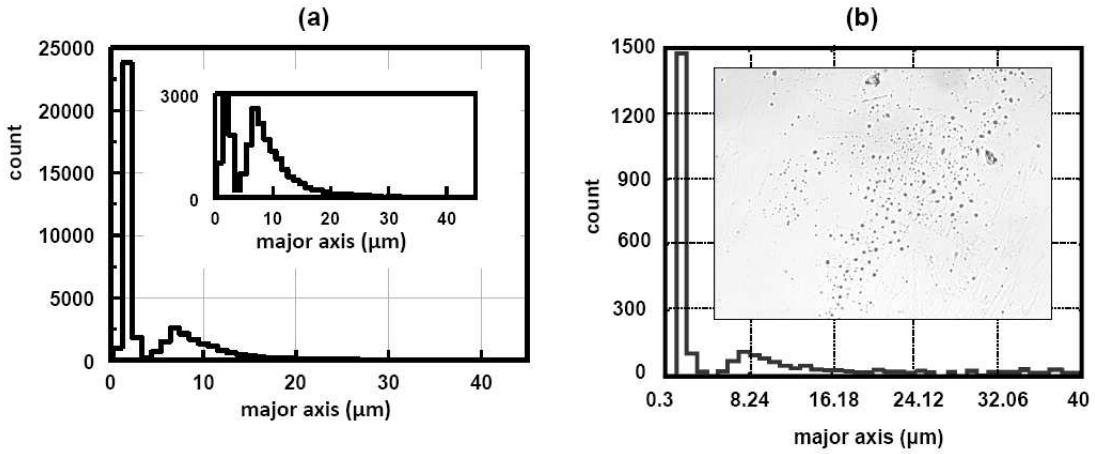

Figure 8. Size distributions measured for the front sides of (a) detector 10-5 used in the SRI immersion experiment (34,254 tracks identified) and (b) our detector used in an 'outside the cell' experiment (2387 tracks identified). A microphotograph of the tracks on the 'outside the cell' detector is shown (200× magnification, field of view is 500 by 600 μm).

respectively. Figure 8b also shows a microphotograph of the tracks obtained at 200X magnification. As can be seen, the image shows that there are large and small tracks as well as both circular and elliptical tracks. The primary difference between the size distributions obtained for both experiments is that there is a more than 90% decrease in energetic particles registered on the detector used in the 'out of cell' experiment. One possible explanation for this observation is that the Mylar film is blocking <0.45 MeV protons, <0.55 MeV tritons, <1.40 MeV ^{3}He, and <1.45 MeV alphas. However, Zhou, a CR-39 detector expert from NASA Johnson Space Center, provided a more plausible explanation that will be discussed below. The size distributions shown in Fig. 8 show two populations of tracks. For both detectors, the majority of the tracks fall between 2 and 3 μm. It should be pointed out that these tracks can only be observed with

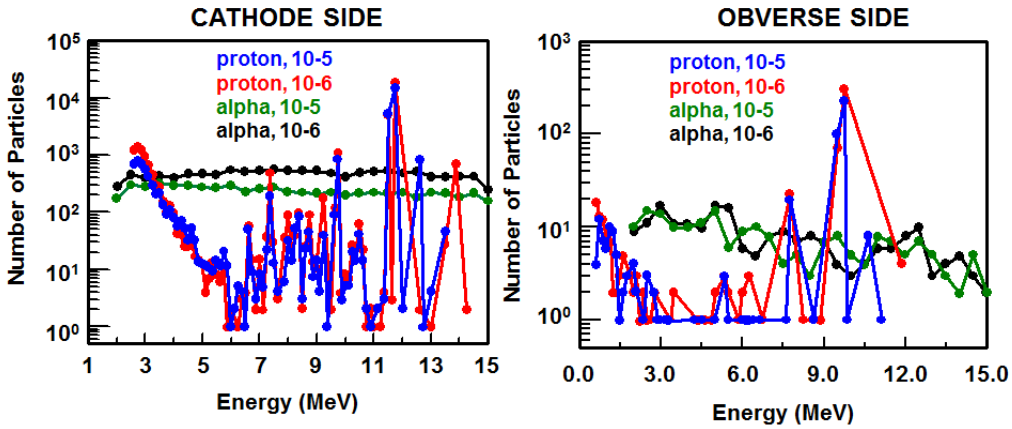

Figure 9. Energy distribution of particles for cathode surface and obverse surface of two CR-39 detectors, designated 10-5 and 10-6, used in immersion experiments. LET analysis was used to determine the energy distributions.

imaging systems using optics that provide highly resolved microphotographs. The second population of tracks extends from 4 μm in diameter all the way out to 40 μm.

For the SRI immersion experiments, the scanner identified tracks on both the front and back surfaces of the detectors. Zhou applied his LET analysis to the scanned data to estimate the energy released by the Pd/D co-deposition generated particles [27]. The specie and energy distribution of the particles are summarized in Fig. 9. The LET analysis spectrally determined that the tracks on the front surface in contact with the cathode were caused by $\geq$1.8 MeV protons, $\geq$1.8 MeV alphas, and secondary particles due to recoils from energetic protons and/or neutrons. On the obverse surface of the detectors, the particles that created the tracks were identified as $\geq$11.8 MeV protons and/or recoils from energetic protons and/or neutrons.

In the immersion experiments done by SRI, there was a 60 μm thick polyethylene film between the Ag/Pd/D cathode and the surface of the CR-39 detectors. The minimum energy needed to pass through the polyethylene film is ~2 MeV for protons and ~8 MeV for alpha particles. From this Zhou [30] concluded that the alpha particles identified on the cathode side of the CR-39 detectors are secondary particles produced by high energy primary protons and neutrons. Consequently the 60 μm polyethylene film acts as a filter, for slower charged particles, and as a neutron or fast proton radiator source of secondary charged particles. If this were the case, the thicker the film, the more secondary particles there will be. To confirm this, an experiment was done using the cathode structure shown schematically in Fig. 10a. The 60 μm polyethylene film covered half of the CR-39 detector. A 6 μm thick Mylar film then covered the entire detector. A Au wire was placed in contact with the covered CR-39 detector. The cathode was immersed in a $PdCl_2$–LiCl–D_2O plating solution and Pd/D co-deposition was done. After completion of the experiment, the detector was etched. Few pits were observed on the Mylar only half of the CR-39 detector. However, a significant number of pits were observed on the polyethylene film side, Figs. 10b and c.

3. Alternative Interpretations of Pd/D Co-deposition Cr-39 Results

3.1. 1 Pits are the result of chemical damage by deuteroxide ions

Oriani asserted that the pits observed in the CR-39 detectors used Pd/D co-deposition experiments were primarily artifacts due to chemical attack by electrolytically generated deuteroxide ions [31]. He argued that these ions etch into the plastic of the detector creating pits. If this were the case, pits would have been observed in the Pd/D co-deposition experiments done on Ni screen in the absence of an external magnetic/electric field described *vide supra*. Likewise pitting would have been observed in the Cu/Ni screen electrolysis experiments in LiCl–D_2O solution and in the Cu/D and Ni/D plating control experiments. Since no pitting was observed in these control experiments, which also produce

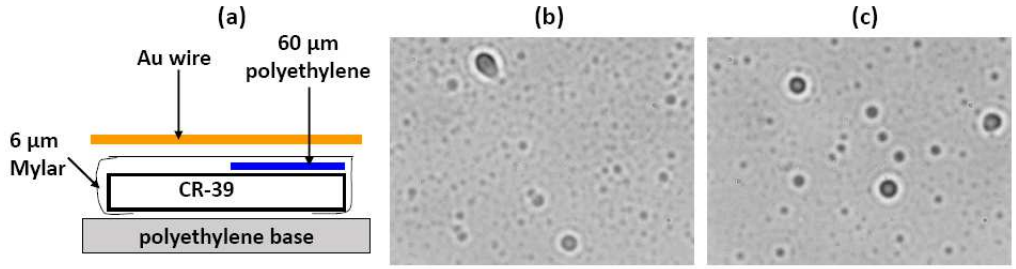

Figure 10. (a) Schematic of a Au cathode used in a Pd/D co-deposition experiment. (b) and (c) Photomicrographs of tracks observed under the 60 μm thick polyethylene film. A magnification of 1000$\times$ was used to obtain the images.

deuteroxide ions, then the pits observed in Pd/D co-deposition are not the result of chemical attack by these ions. Furthermore, the experiments done with the 60 μm thick polyethylene film between the cathode and the detector still showed pitting. This polyethylene film would have protected the detector from chemical attack by deuteroxide ions.

Additional experiments have shown that it is possible to differentiate the features due to chemical attack from those due to energetic-particle generated pits. In our experiments we use Fukuvi brand CR-39, which is a harder form of CR-39 and is more resistant to mechanical and chemical attack. TASL brand CR-39 is softer with a higher neutron detection efficiency. An external magnetic field, Pd/D co-deposition experiment was done with an Ag wire in contact with the TASL-brand CR-39 detector [10]. After etching, visual inspection of the detector showed that it was clear where the cathode had been in close contact with it. The rest of the detector was frosty white in appearance. Results of microscopic examination of the detector are summarized in Fig. 11. In Fig. 11a, a line delineates the transition from the cloudy area and the region that was in contact with the Pd deposit. Figure 11b and c shows images taken in the cloudy and clear areas, respectively. Where the deposit was in contact with the detector, dark circular pits are observed. Bright spots are observed when focusing deeper into the pits. These features are consistent with what is observed for nuclear particle generated pits. The cloudy area shows irregularly shaped, cauliflower-like features that are shallow and show no optical contrast. These features are the result of chemical damage due to electrolysis. These results show that CR-39 from some suppliers are more susceptible to chemical damage than others and is related to the amount of cross-linking in the polymer.

Oriani [31] also questioned our interpretation of the triple tracks. He claimed that he had seen triple, quadruple, and quintuple tracks in CR-39 detectors used in in his experiments. He further said, "It's not enough to see three tracks from one point and jump to the conclusion that that's the disintegration of carbon-12." To our knowledge, Oriani had not exposed CR-39 detectors to a DT neutron source, which is what we did. As discussed *vide supra*, Fig. 6 shows a side-by-side comparison of Pd/D co-deposition and DT neutron generated triple tracks. The tracks look identical and this comparison provides support for our interpretation.

3.2. Pits are the result of chemical damage by oxygen

Shanahan [32] has strongly suggested that O_2 attack is the cause of the pitting observed in the Pd/D co-deposition experiments. He asserts that this could be tested by "bubbling fine O_2 bubbles from a glass frit over CR-39 under otherwise identical experimental conditions." The Cu and Ni electroplating experiment described above fits this criterion and shows that O_2 attack is not the source of the observed tracks in the Pd/D co-deposition system. In addition electrolysis experiments have been done with just Ni or Cu screen used as the cathode [9]. No electroplating of Pd was done in these experiments. The bare Ni/Cu electrolysis experiments ran the same amount of time as the Pd/D

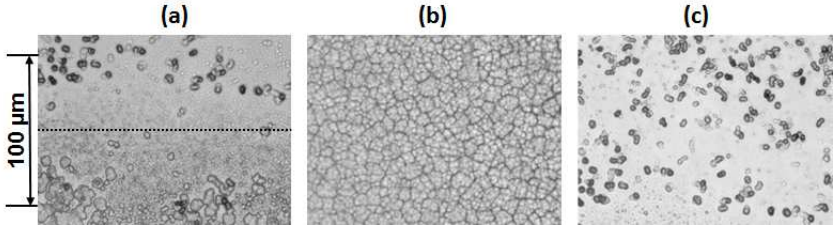

Figure 11. Photomicrographs obtained of TASL CR-39 used in a Pd/D co-deposition experiment in the presence of an external magnetic field. Magnification is 500×. (a) Image taken at the interface where the area above the dotted line was in contact with the cathode and Pd deposit. The area blow the dotted line is outside the cathode. (b) Image taken of a cloudy area that was not in contact with the cathode. (c) Image taken of an area in direct contact with the Pd deposit.

co-deposition experiments. Vigorous D_2 gas evolution was observed in these experiments. After etching, no tracks above background were observed. These experiments indicated that the tracks were not due to O_2 attack nor were they due to the impingement of D_2 gas bubbles on the surface of the detector.

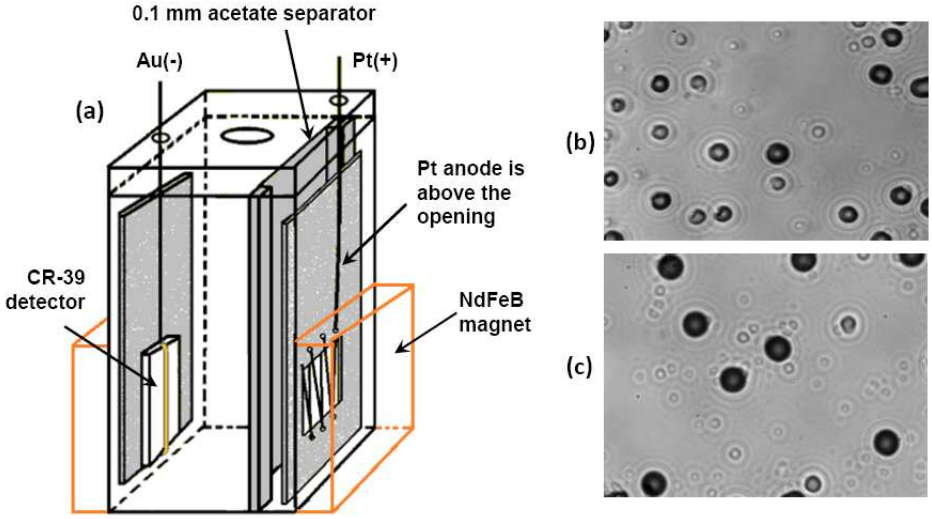

Figure 12. (a) Schematic of the two chamber cell used to separate the anode and cathode. When plating was complete the magnets were placed outside the cell as shown. (b) and (c) Photomicrographs obtained on the front and back surfaces, respectively, of the CR-39 detector used in the two chamber cell experiment. Images were taken at 1000× magnification.

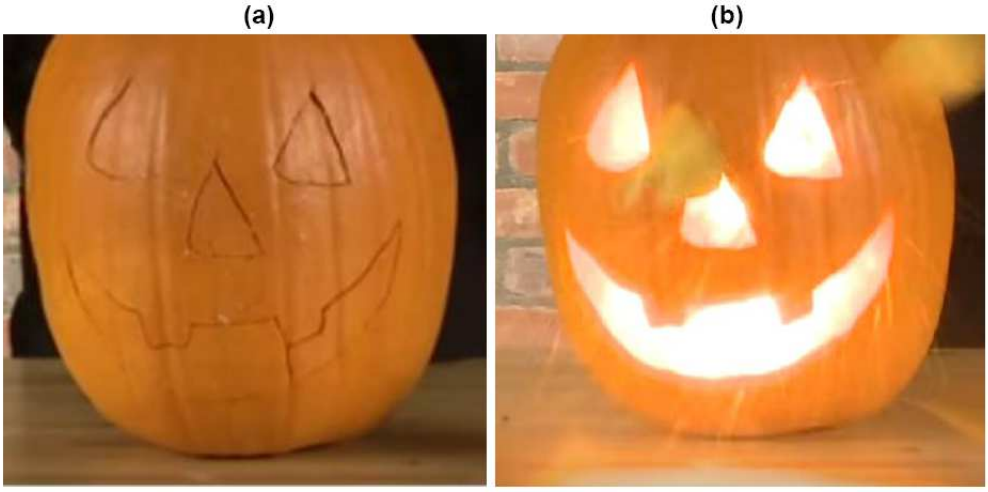

Figure 13. Photographs of a pumpkin obtained (a) before and (b) after a calcium carbide acetylene explosion [38].

An experiment has been done using a two chamber cell that separated the anode and cathode. Figure 12a shows a schematic of the cell. This cell was used in an external magnetic field experiment. External magnets were placed outside the cell when Pd plating was complete. There is a small gap at the bottom of the anode chamber which allows the flow of current. The Pt anode was positioned above this gap. The purpose of this experiment was to impede the mixing of D_2 and O_2/Cl_2 gases generated at the cathode and anode, respectively. The evolution of Cl_2 gas only occurs during the plating phase of the co-deposition process. Tracks in CR-39 were obtained on both the front and back surfaces of the detector, Figs. 12b and c, respectively. The front tracks corresponded with the placement of the Au cathode and the Pd deposit. These experiments provide further evidence that the tracks obtained as a result of Pd/D co-deposition are not the result of O_2 attack.

3.3. Pits are due to shockwaves from D_2/O_2 recombination

A second suggestion of Shanahan's to explain the observed pits in CR-39 is that they are caused by shock waves resulting from D_2/O_2 recombination on the Pd surface [32]. As indicated *vide supra*, CR-39 detectors have been used in ICF [1,2]. In ICF, a laser with a focused intensity on the order of 10^{25} W/m^2 and a pulse length on the order of 10 ns interacts with a dense plasma target containing fusion fuel [33]. This dense target is formed by the implosion of a spherical shell containing cryogenically frozen DT. When intense short-pulse laser beams interact with high density plasmas, strong shock waves result. These shock waves have not caused any damage to the CR-39 suggesting that Shanahan's explanation for the pitting in CR-39 is unlikely. However, unless ameliorated, target disassembly debris from ICF implosions will ablate the inside of the target chamber creating kinetically energetic particles [34]. Without collectors or some other mitigating engineering solution, these fast particles would damage the CR-39 detectors should they reach them. This has most recently been demonstrated by students at Point Loma Nazarene University (PLNU) [35–37]. In 2019 Karahadian and Doss [35] reported that they had done metal deposition experiments using CR-39 detectors. They observed tracks on the detectors when experiments were done using Pd/D co-deposition but no tracks in Cu/D deposition. In 2020, Karahadian et al. [36] reported on the results of 'track' formation resulting from an exploding pumpkin experiment. In this experiment, they placed a CR-39 detector in a cup containing finely granulated calcium carbide. This cup was then placed inside a carved pumpkin. Water was added to the calcium carbide to create acetylene gas, which was then ignited. Figure 13 shows photographs of a pumpkin before and after ignition of the acetylene [38]. It can be seen that the resultant explosion is violent and has blown out the cutouts of the eyes, nose, and mouth of the pumpkin. Not surprisingly, the detector showed pitting and scratches [36,37]. Karahadian et al. [36,37] concluded that the pitting they observed as a result of the exploding pumpkin experiment was similar to those observed as a result of Pd/D co-deposition. They further concluded that the pitting was caused by shockwaves resulting from the explosion. They did not take into account the proximity of the detector to the calcium carbide which, upon ignition, would have sent hot projectiles into the detector that would cause damage. At best this experiment shows how much energy is required to cause pitting in CR-39 detectors. It needs to be emphasized that control experiments need to reflect the chemical and electrochemical reactions occurring inside an electrolytic cell and this particular experiment did neither.

Experience has shown that once the Pd deposit is wet, recombination of theD_2 and O_2 does not occur. In these experiments, the Pd deposit was completely immersed in the solution. Consequently, it is unlikely thatD_2/O_2 recombination is occurring. However, our experimental results discussed above provide additional support that the pitting observed in CR-39 detectors is not due D_2/O_2 recombination shock waves as the source of the pitting observed in the detectors. As indicated *vide supra*, tracks have been observed on both the front and back surfaces of CR-39 detectors used in Pd/D co-deposition experiments [10]. The CR-39 detectors are 1 mm thick. It is difficult to explain how a shockwave from a mini-explosion occurring on the front surface of the detector can propagate itself to cause pitting on the back surface without obliterating the detector. In the SRI replication [27], a 60 μm polyethylene film was between

the cathode and the detector. This film will protect the detector from damage due to D_2/O_2 recombination, should it occur.

We conducted an experiment that took advantage of what was observed for Pd/D co-deposition done on Ni and Ni/Au screen cathodes in the absence of an external electric/magnetic field [39]. It was shown that Pd/D co-deposition done on a Ni screen, in the absence of an external electric/magnetic field, did not show pits but rather an impression of the Ni screen, Fig. 1a–c. However, Pd/D co-deposition on a Ni/Au screen cathode, in the absence of an external electric/magnetic field, did produce pitting, Fig. 3c. An experiment was done using a composite cathode in the absence of an external electric/magnetic field [39]. A photograph of the composite electrode is shown in Fig. 14a. Half of the composite cathode is bare Ni screen. The other half has metallic Au that had been plated on the Ni screen. At the end of the experiment, which was done in the absence of an external electric/magnetic field, the detector was etched and analyzed. The results show that no tracks were obtained on the bare half of the cathode, Fig. 14b. The impression of the Ni screen is observed. However, tracks were obtained on the Au-plated Ni screen, Fig. 14c.

Its needs to be emphasized that both halves of the composite cathode experienced the same chemical and electrochemical environment at the same time. If Shanahan's suppositions were correct that the pitting in CR-39 is caused by either chemical reactions with O_2 or to shock waves resulting from D_2/O_2 recombination, those reactions would have occurred on both the bare Ni and Au-coated Ni halves of the cathode and both halves would have shown pitting of the CR-39 detector. This was not observed.

3.4. Corona discharges are responsible for the pits

Kowalski [40] has suggested that the pitting observed in CR-39 detectors used in Pd/D co-deposition experiments are due to an electrical effect. He said that shallow pits in CR-39 can be created by a 'deliberately induced corona discharge.' What he did not indicate was that this corona discharge experiment had been conducted in air [41]. It is nontrivial to create a corona discharge in an aqueous system. For instance, to degrade organic contaminants, such as phenol in water, 15 kV were needed to create a corona discharge from a 50 μm diameter Pt tip electrode. As solution conductivity increases, higher voltages are required to create a corona discharge. The Pd/D co-deposition experiments are conducted in the presence of an electrolyte, usually LiCl. These solutions are highly conductive. Also the measured cell voltages do not exceed 8 V. Given these conditions, it is highly unlikely that corona discharges were

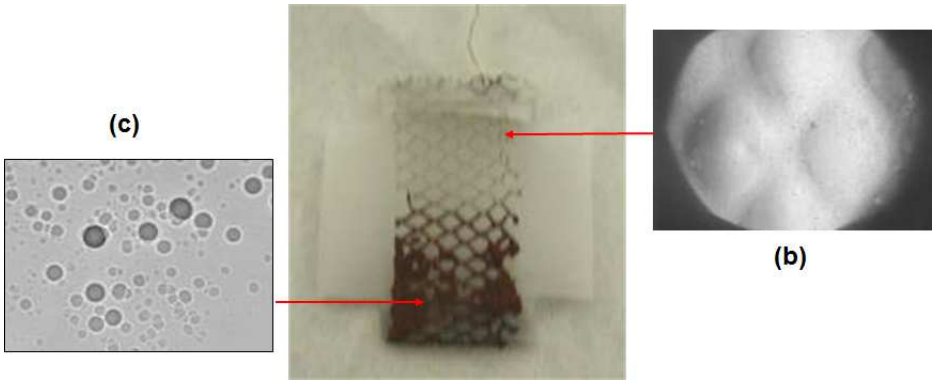

Figure 14. CR-39 results for Pd/D co-deposition done on a composite cathode in the absence of an external electric/magnetic field. (a) A photograph of the composite cathode. (b) Photomicrograph of CR-39 detector in contact with the bare Ni screen half of the composite cathode, 20× magnification. The impression of the Ni screen is observed. (c) Photomicrograph of CR-39 in contact with the Au-plated Ni half, 1000× magnification. Tracks are observed.

created in the Pd/D co-deposition experiments. Finally, if the pits observed in Pd/D co-deposition were indeed due to a corona discharge, such pits would have been observed in the $CuCl_2$ and $NiCl_2$ electroplating experiments discussed *vide supra*. No pits were observed in either the Cu or Ni plating experiments.

Modeling of tracks in CR-39 detectors used in Pd/D co-deposition experiments was done using TRACK_TEST [29]. TRACK-TEST is a computer program developed by Nikezic and Yu that calculates track parameters such as the lengths of the major and minor axes and track depth for alpha particles [42,43]. The computer program also plots the profile for each etch pit in CR-39. When using TRACK_TEST, the input parameters are particle energy, incident angle, etch rate, and etch time. Using this program, the energies of the alpha particles registered on the CR-39 detectors were on the order of 1 MeV [29]. Despite this modeling, Kowalski has said that the Pd/D co-deposition generated tracks are too large to be due to alpha particles [44]. Other researchers have said that the tracks are too shallow to be nuclear generated tracks and have commented that the majority of the tracks are circular in shape and not elliptical and [45,46]. In their critiques, these researchers are not taking into account the linear energy transfer (LET) losses to particles traversing the Pd deposit, cathode wires, and aqueous. It has to be emphasized that we can only estimate the energy of the particle when it impacts the CR-39 detector. This can be significantly less than the energy when the particle was 'born.' Nonetheless, both typical fusion protons (>3–17 MeV) and alphas (>3 MeV), often have sufficient energy to induce tracks in CR-39.

Figure 15a is a schematic describing the layers a charged particle, such as an alpha, has to negotiate before it impacts a CR-39 detector used in a Pd/D co-deposition experiment [29,47]. An SEM of the Pd deposit is shown in Fig. 15a. The deposit has a cauliflower-like morphology that traps pockets of water. Energetic particles can be born anywhere inside the lattice of the Pd deposit. As shown in the schematic in Fig. 15a, after birth, the particles have to pass through the Pd deposit and the water layer before impinging the detector. Figure 15b shows LET curves calculated for protons, tritons, helium-3, and alpha particles in palladium and in water. These LET curves are used to determine

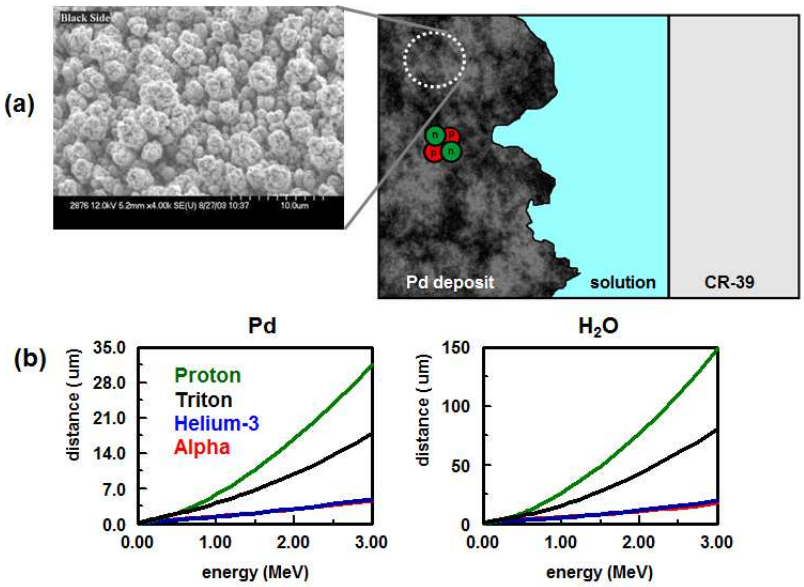

Figure 15. (a) Schematic describing the layers a charged particle has to negotiate before it impacts the CR-39 detector. An SEM of the Pd deposit formed as the result of the co-deposition process is shown. (b) LET curves calculated for charged particles traversing through palladium and water.

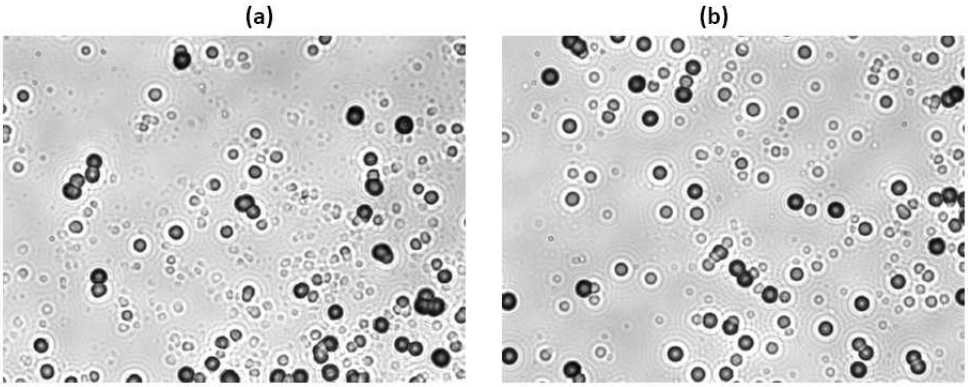

Figure 16. Photomicrographs obtained at 500× magnification for (a) Pd/D co-deposition tracks and (b) 1 MeV alpha tracks.

the magnitude of the effect of Pd and water on the energies of the charged particles. The LET curve for Pd indicates that, in order for particles to be detected by a CR-detector, the particles need to originate near the surface of the Pd. Particles formed deeper inside the deposit will simply not have enough energy to exit the lattice and travel through the deposit and water layer to reach the CR-39 detector. The observed narrow particle energy range suggests the particles are produced at a similar depth within the Pd.

To simulate the effect of water on the transmission of charged particles, layers of Mylar were placed between a CR-39 detector and an ^{241}Am alpha source. Figure 16 shows a side-by-side comparison of Pd/D co-deposition tracks with ~1 MeV alpha tracks formed by placing 24 μ m of Mylar between an ^{241}Am alpha source and a CR-39 detector. The Pd/D and ~1 MeV alpha tracks are indistinguishable. As indicated above, one of the main criticisms raised about the tracks observed in CR-39 detectors used in Pd/D co-deposition experiments is the scarcity of elliptical tracks. As shown in Fig. 16a, the observed tracks are primarily circular in shape. Likewise the ~1 MeV alpha tracks are primarily circular in shape, Fig. 16b. The results in Fig. 16 indicate that only charged particles with trajectories normal to the surface have sufficient energy to get through the water layer, in the case of Pd/D co-deposition, and Mylar, in the case of the ^{241}Am alpha source, to impact the detector. Charged particles traveling at oblique angles are deflected and either do not reach the detector or leave small indentations.

3.5. Why are no Pd X-ray emissions observed during electrolysis?

Hagelstein pointed out that charged particles going through Pd should stimulate Pd K shell X-ray emissions which we had not observed despite CR-39 evidence of MeV charged particles. A literature search showed that others had used lithium drifted silicon, Si(Li), detectors to detect X-ray emissions during Pd/D electrolysis in real time [48,49], however, no X-rays above background were detected. The main difference between the two approaches to detect energetic particles is that CR-39 is a constantly integrating detector while the measurement of X-rays using a Si(Li) detector is done in real time. To address this possible discrepancy, simulation experiments were conducted using a 0.1 μCi ^{210}Po source, a 25 μm thick Pd foil, and a 18% HPGe with a Be window [50]. ^{210}Po is supposed to be a pure alpha source, however our source exhibited three gamma/X-ray lines at 14.4, 21.9, and 121.7 keV from an unknown radionuclide(s) contaminant. While the presence of the contaminant(s) in the ^{21}0Po source was unexpected, it did present an opportunity to separate and quantify the alpha/gamma contributions in stimulating the Pd K shell X-rays. The ^{210}Po source was placed in contact with a Pd foil [50].

3.6. Why are the pits observed in CR-39 shallow and primarily circular in shape?

Spectra were obtained by placing the sample perpendicular to the Be window of the HPGe detector, Fig. 17a-i, and directly facing the detector, Fig. 17a-ii. The perpendicular orientation is representative of the cathode arrangement used in some of our electrolysis experiments. No Pd K shell X-rays were observed with the ^{210}Po–Pd sample perpendicular to the detector. However, when the Pd foil and ^{210}Po source were facing the Be window of the HPGe detector, the Pd Kα line at 21.1 keV was observed as was the 21.9 keV line due to the contaminant in the ^{21}0Po source. Consequently, the orientation of the cell relative to the HPGe detector will determine whether or not Pd X-ray emissions will be detected. Photoabsorption is another factor that determines the likelihood of observing Pd K shell X-ray emissions [50]. The thicker the Pd cathode, the more these X-rays are absorbed. For –300 μm Pd foils, the percentage of Pd X-rays absorbed is 12.2–99.3. There will also be attenuation of the Pd X-rays by the components of the cell. As a worse case scenario, we will assume that experimental conditions are ideal and will ignore the impacts of cell orientation, photoabsorption, and attenuation by cell components on the detectability of Pd K shell X-ray emissions.

Figure 17b shows time-normalized spectra of (i) the Pd foil, (ii) ^{210}Po source, (iii) Pd foil in contact with ^{210}Po source, and (iv) a 100 μm thick acrylic film is between the Pd foil and the ^{210}Po source [50]. The acrylic film will block the alphas from the ^{210}Po but not the gammas from the unknown contaminant(s). All spectra were obtained in a Pb cave lined with Sn and Cu foils to reduce the Pb fluorescence. The samples were in direct contact with the HPGe detector. The regions of the gamma lines of the unknown contaminant(s) are indicated as well as the Pd K shell line at 21.1 keV. In Fig. 17b-i, a small peak due to the Pd α shell X-ray line is observed. The fluorescence from the Pb bricks of the cave is stimulating the Pd Kα shell X-ray emission. The spectrum obtained for the ^{210}Po source is shown in Fig. 17b-ii. The gamma lines due to the unknown contaminant(s) are observed at 14.4 and 21.9 keV. Figure 17b-iii is the spectrum obtained when the ^{210}Po source is in contact with the Pd foil. The Pd K-shell emissions are stimulated

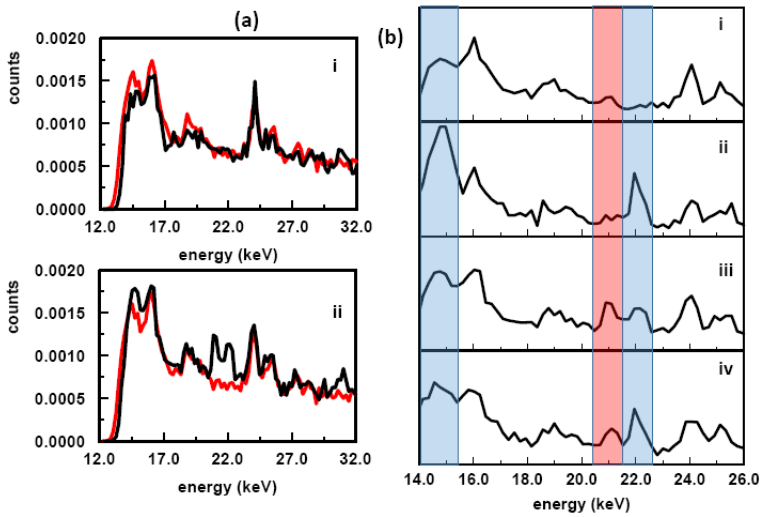

Figure 17. (a) Time–normalized gamma ray spectra obtained with the ^{210}Po–Pd sample oriented perpendicular to the detector window, i, and facing the detector window, ii. Background and sample spectra are red and black, respectively. (b) ^{210}Po–Pd experiments conducted by placing the samples in a Pb cave and in direct contact with the HPGe detector where: i = Pd foil, ii = ^{210}Po source, iii = Pd foil in contact with ^{210}Po source, iv = a 100 μm thick acrylic film is between the Pd foil and the ^{210}Po source. Spectra are time-normalized. The blue bars indicate the gamma lines of the unknown contaminant(s) and the red bar indicates the Pd Kα shell X-ray.

Table 2. Measured intensities of the Pd Kα line in the spectra shown in Fig. 17b [50].

Sample[a]	Intensity of the Pd Kα line[b]	Cause of stimulation[c]
^{210}Po source	0.00	None
Pd foil	1.9×10^{-4}	bkg
^{210}Po-Pd foil	5.4×10^{-4}	bkg $+ \alpha + \gamma$
^{210}Po-acrylic film-Pd foil	3.0×10^{-4}	bkg $+\gamma$

a All samples were measured in a Pb cave lined with Sn and Cu foils.
b Spectra have been time-normalized.
c bkg = background stimulation, α = stimulation by alphas from the ^{210}Po source, γ = stimulation by the gamma rays from the contaminant(s) in the ^{210}Po source.

by the lead cave background, the^{210}Po alphas, and the gamma rays from the unknown contaminant(s) as evidenced by the decrease in the intensities of the contaminant(s) gamma lines at14.4 and 21.9 keV. The spectrum resulting from placing the acrylic film between the Pd foil and ^{210}Po source is shown in Fig. 17b-iv. Because the ^{210}Po alphas are blocked, the Pd Kα X-ray peak is less intense than in Fig. 17b-iii.

By comparing the intensities of the Pd Kα shell X-ray line in the spectra shown in Fig. 17b and assuming that the sources of the Pd X-ray stimulation contribute additively, it is possible to estimate the contributions of each source. Table 2 summarizes the measured intensities of the Pd Kα lines in Fig. 17b. From these measurements, the estimated contributions of each source in stimulating the Pd X-ray emissions are 35.2% due to background, 44.4% due to the ^{210}Po alphas, and 20.4% due to the unknown contaminant(s) gamma/X-rays.

The results of the ^{210}Po–Pd foil experiments can be used to determine whether or not Pd K shell X-rays should have been observed in the Pd/D co-deposition experiments under ideal experimental conditions [50]. The ^{210}Po alpha source used in these experiments has an activity of 0.1 μCi. This activity is equivalent to 3700 decays/s. For the time normalized spectra shown in Fig. 17b-iii, 3700 alpha particles are stimulating Pd K shell X-rays. The peak due to the Pd Kα X-ray in the spectrum for the Pd foil in the Pb cave, Fig. 17b-i, does not overlap with the peak due to the contaminant in the ^{210}Po source. Consequently, the area of the Pd Kα X-ray peak can be accurately measured and is 9.22×10^{-5}. The analysis discussed above indicated that 44.4 % of the Pd X-ray peak intensity/area is due to alpha particle stimulation and 20.4% is due to stimulation by the fluorescence background of the cave. Therefore, the peak area due to stimulation by 3700 alpha particles is 1.163×10^{-4}.

Figure 18a shows a photomicrograph of tracks obtained by scanning a CR-39 detector used in a Pd/D co-deposition experiment. The automated system does computer processing to identify and number objects in the scanned image,

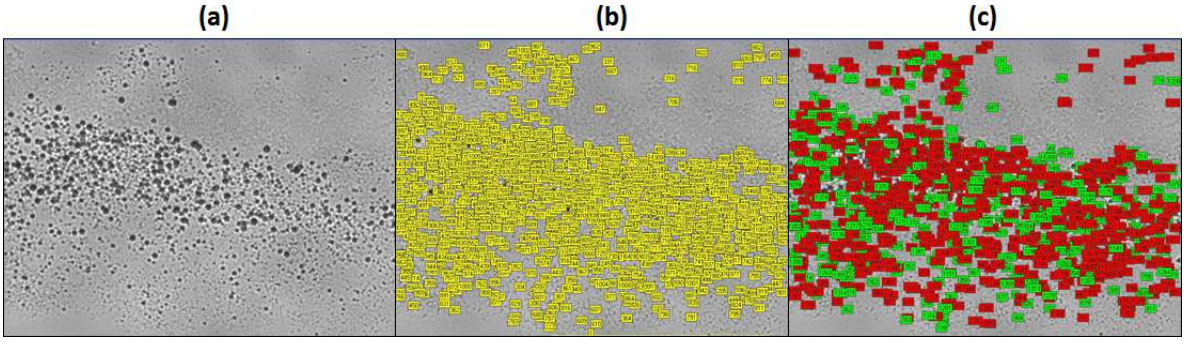

Figure 18. Results of scanning a CR-39 detector detector used in a Pd/D co-deposition experiment: (a) raw image obtained at a magnification of 200×, (b) objects identified in image (a), (c) after processing, positively identified tracks are green and non-tracks are red.

Fig. 18b. Based upon measurements of object symmetry and contrast, the computer algorithm identifies pits whose properties are consistent with those of nuclear generated tracks. The software algorithm ignores overlapping pits. Positively identified tracks are indicated by green rectangles, Fig. 18c. A 1 mm x 20 mm area of the CR-39 detector shows that 1079 tracks were positively identified. Since overlapping pits are discarded, the number of tracks in Fig. 18a is estimated to be undercounted by a factor of 3. Since the total area of the detector is 10 mm x 20 mm, at a minimum, the number of tracks is undercounted by a factor of 30. For this scenario, it is assumed that the observed tracks are due to charged particles and not neutrons. Charged particle stimulation of the Pd K shell X-rays will occur throughout the Pd deposit. Ignoring photoabsorption of the 22 keV Pd K shell X-rays by the Pd deposit and cell components, we estimate charged particles are undercounted by another factor of 1000. In this worst case scenario, the total number of charged particles in 3.237x107. For a two week experiment (1.2096x1^{06} s), the rate of particle production is estimated to be 26.8 particles/s. he increase in peak area of the Pd Kα X-ray line by 26.8 charged particles, in the time normalized spectrum, is calculated to be 8.42x1^{0-}7. This would be too small an increase in peak area to see in the measured spectrum.

3.7. Anomalous and overlapping tracks

High track density affects the bulk vs track etch rates. Areas of high track density are ignored when manually measured and *defacto* ignored by automated scanners. Manual counting indicated >104 tracks/m^{m2}, where the tracks were distinct. Uncounted, high density areas likely exceed this by 1–2 orders of magnitude. However, Ghazaly and Hassan [51] found experimentally that both fast protons and alphas also increase the bulk CR-39 etching rate. Although this was performed with TASL CR-39, which is softer than the preferred Fukuvi for Pd/D co-deposition, similar effects can be expected. The author' Figs. 3–H and 4E–H, of high fluence alphas reproduced in Fig. 19a and b, show etched tracks identical to Pd/D Co-deposition high density tracks, examples shown in Fig. 19c. In particular, image F in Fig.

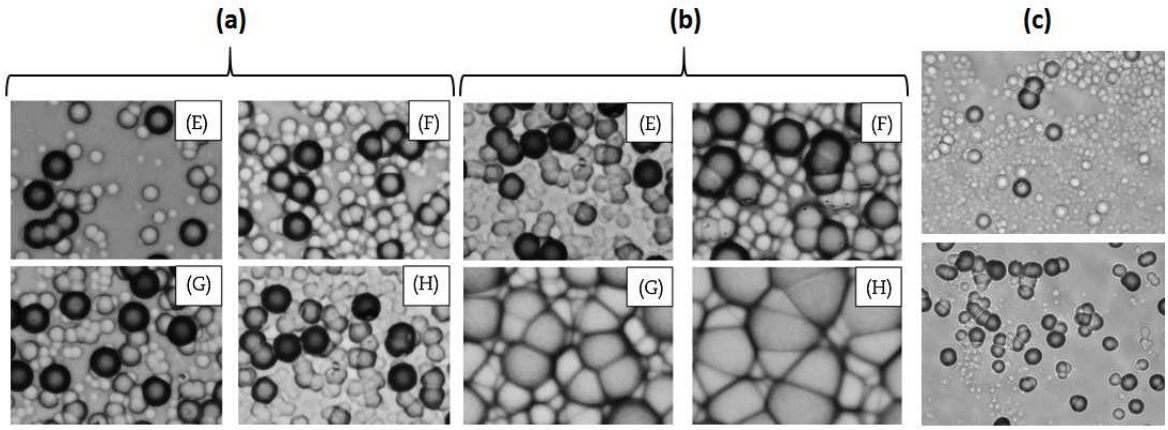

Figure 19. Photomicrographs of tracks in CR-39 detectors where (a) is Fig. 3E–H [51], (b) is Fig. 4E–H [51], and (c) is from Pd/D co-deposition experiments. For Fig. (a) the CR-39 detector was irradiated with a different fluence of alpha particles where $E = 1.47 \times 108$, $F = 4.05 \times 108$, $G = 5.30 \times 108$, and $H = 7.36 \times 108$ alphas/cm^2. The detector was etched for 4 h in 6.25N NaOH at 70°C. For Fig. (b) the CR-39 detector was irradiated with 1.5 MeV alpha particles at a fluence of 7.36×108 alphas/cm^2. The detector was etched in 6.25N NaOH at 70°C for different etching times where $E = 4$, $F = 6$, $G = 10$, and $H = 14.5$ h. For Fig. (c), The CR-39 detectors were used in Pd/D co-deposition experiments done on a Ag wire in the presence of an E field (*top*) and B field (*bottom*). The detectors were etched in 6.5 N NaOH at 62–65°C for 6 h. Images were obtained at 500× magnification. Figures (a) and (b) are reprinted with permission from Elsevier.

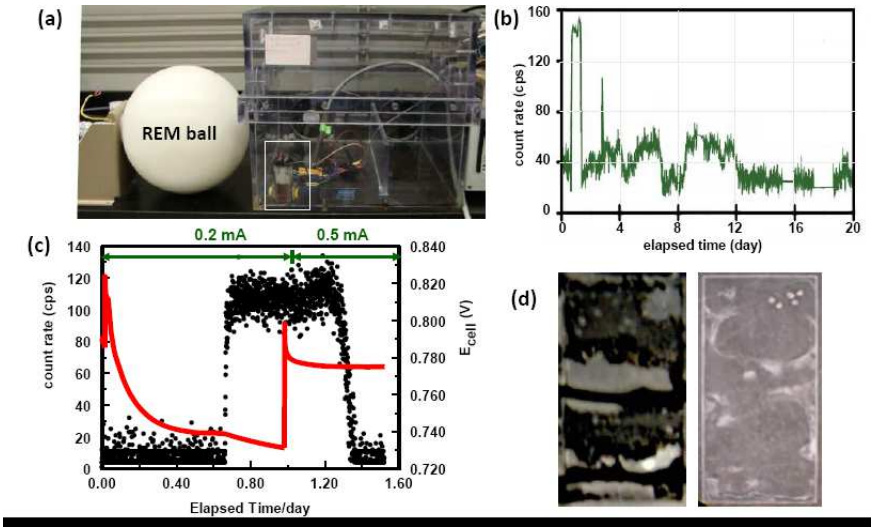

Figure 20. Summary of real-time neutron measurements done during the SRI replication done in 2006 where (a) photograph of the cell (indicated by a white square) and the REM ball/BF3 detector outside the acrylic chamber, (b) neutron count rate as a function of time, and (c) neutron count rate and cell voltage measured during the large neutron excursion on day one. (d) Photograph of the front surface of the polyethylene cover and CR-39 detector used in an immersion experiment.

19b has a TASL etch time of 6 h at 7°C using 6.25 M NaOH etchant. This is similar to Pd/D co-deposition Fukuvi etching parameters. The authors used a 1.5 MeV alpha fluence of 7.36 $\times 10^8$ tracks/c^{m2} to obtain this image. This is identical to the track density and anomalous features observed during co-deposition, Fig. 19c.

Consequently, at very high charged particle fluences, tracks will more easily overlap as the track and bulk etch rates also converge, and also present poorly formed tracks. Nonetheless, this study [51] indicates that high charged particle fluxes with known alphas are consistent with co-deposition track formation. Indeed, due to the converging bulk, $_{\mathrm{Vb}}$ and track, $_{\mathrm{Vt}}$, etching rates, co-deposition fluxes are orders of magnitude higher than reported

These authors [51] note various filters have been employed to reduce the number of particles reaching the CR-39, in which case the LET losses through the filter can be accounted for via the SRIM/TRIM modeling codes. The use of step-ranged (SRF) and Si-wedged range filters (WRF) with CR-39 are commonly used in inertial confinement fusion for proton spectroscopy [19,52]. We note similar filtering in Section 3.3 where a 60μm protective barrier on the detector was used during co-deposition

3.8. Real-time measurements vs. CR-39

Earlier we wrote a review of LENR studies that had used CR-39 detectors [53]. In this paper we indicated that, compared to electronic, real-time detectors, solid state nuclear track detectors were ideal for use in LENR experiments and enumerated a number of advantages including the fact that they can be placed in close proximity to the cathode eliminating solid angle losses, they are not affected by low level electronic noise, are constantly integrating, and do not require expensive and complicated electronic modules for both timing and background discrimination. Despite this we have been told that one cannot take the CR-39 results seriously without commensurate real-time measurements.

One problem with real-time detectors is that they cannot be immersed inside electrolytic cells and must be placed outside the cell. Often configurations that are ideal for real-time measurements are not ideal for electrolysis. This was

demonstrated in a Pd/D co-deposition experiment we conducted using a silicon surface barrier (SSB) detector to detect charged particles in real-time [53]. A 6 μm thick Mylar window separated the Au wires from the detector. To decrease scattering, a 100 μm thick acrylic collimator was placed outside the Mylar window. Given the geometry of the cell, it was not possible to place a CR-39 detector inside as it would have impeded current flow between the anode and cathode. The assembled cell was filled with plating solution and placed on top of the SSB detector. When a current was applied to the cell, an increase in the number of counts was observed. However, these counts decreased overnight. LET analysis indicated that this decrease was not surprising. As Pd plates out, the growing Pd deposit will prevent charged particles from leaving the cell and entering the detector.

Another problem with real-time measurements was partially addressed in the discussion in Section 3.6 as to why no Pd X-rays were observed as energetic charged particles were generated. Given the size of the cells typically used in Pd/D co-deposition experiments and ignoring photoabsorption and cell geometry, the rate of particle generation was too low to see an observable change in the X-ray spectrum. Two ways to increase the generation rate are to either use larger cells or to use multiple cells. The later was demonstrated by the earlier SRI replication described *vide supra* [27,28]. Besides CR-39, a BF_3 neutron detector was used to monitor the two cells used in the immersion experiments [54]. Figure 20a is a photograph of the orientation of the detector relative to the two electrolytic cells inside a protective, acrylic chamber. The BF_3 detector has a polyethylene REM ball (the white sphere shown in the photograph). The REM ball moderates the neutrons, slowing them down for capture by ^{10}B. The neutron count rate as a function of time is shown in Fig. 20b. Several bursts of neutrons were observed during the twelve days of operation. Figure 20c shows plots of the neutron count rate and cell voltage, superimposed upon one another, measured during the large neutron excursion that occurred on day one of cell operation [55]. It can be seen that, as the neutron count rate increased, a simultaneous decrease in the cell voltage occurred. Such decreases in cell voltage are indicative of heat production. There is an apparent discrepancy in the BF_3 neutron count rate and the neutron count rate estimated from the sequential etching analysis of the CR-39 detectors [54]. One explanation offered for this discrepancy was that the signal from the BF_3 detector contained a significant electromagnetic noise fraction induced by the electrolysis power supply. This was highly unlikely as detectors of this type have been used in other environments where the electronic background is much higher. Another explanation was that the response of the BF_3 detector was affected by moisture. We asked Dr. Richard Kroeger, an astrophysicist at SPAWAR Systems Center Pacific in charge of the RADIAC group with vast experience on nuclear detectors, if he knew of any moisture problems with ^3He and BF_3 neutron counters. His response was:

Moisture internal to the counter – never, but it would kill it.

Moisture in and around the HV circuitry – noise or worse.

Moisture in the universe – more thermals for everyone!

Since it is unlikely that the discrepancy between the CR-39 and BF_3 detector is due to instrument malfunction caused either by moisture or electromagnetic noise, it must be due to the manner in which the CR-39 detector was analyzed. As shown in Figs. 2, 3e, 7a, and 18a, a high density of tracks occur where the Pd deposit was in contact with the detector. In these regions the detector has become saturated and direct track counting is not possible as discussed in Section 3.7. In this regime, optical measurements of saturated CR-39 detectors become unreliable, since the optical response of the saturated detectors with respect to the ion?uence is highly nonlinear [56]. Lipson et al. [54] had indicated that, in their analysis, they ignore these regions. Figure 20d shows photographsof the 60 μm polyethylene film that covered the detector and the etched CR-39 detector obtained at the end of an immersion experiment. The polyethylene cover shows where the Pd deposit was in contact with the detector. The etched detector shows several high density track areas, which would also be areas of high activity. By ignoring these areas it is quite probable that Lipson et al. have greatly undercounted tracks resulting from neutrons and that the CR-39 and BF3 detectors may actually be in agreement.

4. Conclusions

We have addressed questions and critiques regarding using CR-39 in Pd/D co-deposition. There have been questions on the nuclear origin of the tracks. However, using a bare Ni, Au-plated Ni screen composite cathode in a Pd/D co-deposition experiment, it was demonstrated that the observed pitting in CR-39 detectors were not the result of chemical damage by either deuteroxide or oxygen attack nor are they due to shock waves resulting from D_2/O_2 recombination or corona discharges. There have been questions as to why the Pd/D co-deposition tracks are predominantly circular in shape. LET curves for charged particles in Pd metal and water showed that only particles traveling perpendicular to the CR-39 detector have sufficient energy to impact the detector. As a result, the tracks are primarily circular in shape. It has been noted that charged particles traversing through a metal should stimulate K shell X-rays that are not observed. Using a ^{210}Po source, it was shown that the experimental configuration determined whether or not X-rays would be seen. It was also shown that the rate of charged particle production was too low to detect measureable Pd K shell X-ray emissions. Furthermore photoabsorption of the X-rays by the Pd deposit and cathode substrate as well as attenuation of the X-rays by components in the cell will further decrease the likelihood of measuring these X-rays in real-time. Attenuation was also a problem in real-time measurements of charged particles using a SSB detector. Given the configuration of the cell, it was not possible to simultaneously use CR-39 and the SSB detector in the experiment. We also did an analysis of the SRI immersion experiments that used both CR-39 and a BF3 detector to monitor the cells in real-time. By ignoring the over saturated regions in the CR-39 detectors, the number of neutrons was significantly under counted and that both detectors were likely in agreement.

References

[1] J.A. Frenje, C.K. Li, F.H. Séguin, D.G. Hicks, S. Kurebayashi, R.D. Petrasso, S. Roberts, V.Yu. Glebov, D.D. Meyerhofer, T.C. Sangster, J.M. Soures, C. Stoeckl, C. Chiritescu, G. J. Schmid, R.A. Lerche, Absolute meaurements of neutron yields from DD and DT implosions at the OMEGA laser facility using CR-39 track detectors, *Rev. Sci. Instrum*. 2002, **73**, p. 2597.

[2] F.H. Séguin, J.A. Frenje, C.K. Li, D.G. Hicks, S. Kurebayashi, J.R. Rygg, B.-E. Schwartz, R.D. Petrasso, S. Roberts, J.M. Soures, D D. Meyerhofer, T.C. Sangster, J.P. Knauer, C. Sorce, V. Yu. Glebov, Spectrometry of charged particles from inertial-confinement-fusion plasmas, *Rev. Sci. Instrum*. 2003, **74**, p. 975.

[3] X.Z. Li., The precursor of cold fusion phenomenon in deuterium/solid systems, in *Anomalous Nuclear Effects in Deuterium/Solid Systems*, AIP Conference Proceedings, New York, 1990, p. 228.

[4] A.G. Lipson, B. F. Lyakhov, A. S. Roussetski, T. Akimoto, T. Mizuno, N. Asami, R. Shimada, S. Miyashita, A. Takahashi, Evidence for low-intensity D-D reactions as a result of exothermic deuterium desorption from Au/Pd/PdO:D heterostructure, *Fus. Technol*. 2000, **38**, p. 238.

[5] A.S. Roussetski. Application of CR-39 plastic track detector for detection of DD and DT-reaction products in cold fusion experiments, in 8^{th} *International Conference on Cold Fusion,* Italian Physical Society, Bologna, Italy, 2000.

[6] A.G. Lipson, A.S. Roussetski, G.H. Miley, and E.I. Saunin, 'In-situ charged particles and X-ray detection in Pd thin film-cathodes during electrolysis in Li2SO4/H2O,' in *Condensed Matter Nuclear Science: Proceedings of the 9th International Conference on Cold Fusion* (Tsinghua Univ. Press, Beijing, 2002).

[7] A.S. Roussetski, A.G. Lipson, B.F. Lyakhov, and E.I. Saunin, 'Correct identification of energetic alpha and proton tracks in experiments on CR-39 charged particle detection during hydrogen desorption from Pd/PdO:H_x heterostructure,' in *The 12th International Conference on Condensed Matter Nuclear Science* (Yokohama, Japan, 2005).

[8] A.G. Lipson, A.S. Roussetski, G.H. Miley and E.I. Saunin, Phenomenon of an energetic charged particle emission from hydrogen/deuterium loaded metals, In *Condensed Matter Nuclear Science: Proceedings of the 10th International Conference on Cold Fusion* ed. P.L. Hagelstein and S.R. Chubb (World Scienti?c, Singapore, 2006)

[9] P.A. Mosier-Boss, S. Szpak, F.E. Gordon, L.P.G. Forsley, Use of CR-39 in Pd/D co-deposition experiments, *Eur. Phys. J. Appl. Phys*. 2007, **40**, p. 293.

[10] P.A. Mosier-Boss, S. Szpak, F.E. Gordon, L.P.G. Forsley, Detection of energetic particles and neutrons emitted During Pd/D co-deposition, in *Low-Energy Nuclear Reactions Sourcebook Volume 1*, ed. J. Marwan and S. Krivit (American Chemical Society, Oxford University Press, Washington, D.C., 2008).
[11] M. Miles, B.F. Bush, J.J. Lagowski, Anomalous effects involving excess power, radiation, and helium production during $_{D2}$O electrolysis using palladium cathodes, *Fusion Technol*. 1994, **2**5, p. 478.
[12] S. Szpak, P.A. Mosier-Boss, J.J. Smith, On the behavior of Pd deposited in the presence of evolving deuterium, *J. Electroanal.Chem*. 1991, **30**2, p. 255.
[13] S. Szpak, P.A. Mosier-Boss, J.J. Smith, On the behavior of the cathodically polarized Pd/D system: search for emanating radiation, *Phys. Lett. A* 1996, **210**, p. 382
[14] V. Violante, P. Tripodi, D. Di Gioacchino, R. Borelli, L. Bettinali, E. Santoro, A. Rosada, F. Sarto, A. Pizzuto, M.C.H. McKubre, F. Tanzella, X-ray emission during electrolysis of light water on palladium and nickel thin films, in *The 9th International Conference on Cold Fusion, Condensed Matter Nuclear Scienc*e, *Tsinghua Univ., Beijing* (Tsinghua Univ. Press, China, 2002)
[15] Z.A. Tayyeb, Use of CR-39 polymer for radiation dosimetry, *JKAU: Eng. Sci*. 2011, **2**2, p. 79
[16] K.M. Thabayneh, M.Y. Shoeib, Studying some properties of CR-39 detector under the effect of different gamma doses, *JAAUBAS* 2016, **2**0, p.55.
[17] D. Evans, Swelling and gas evolution in irradiated organic matrix composites– a review, in *Advances in Cryogenic Engineering: Transactions of the Cryogenic Engineering Conferenc*e, ed. U. Balachandran (American Institute of Physics, 2010).
[18] D.T. Casey, J.A. Frenje, F.H. Séguin, C.K. Li, M.J. Rosenberg, H. Rinderknecht, M.J.-E. Manuel, M. Gatu Johnson, J.C. Scharffer, R. Frankel, N. Sinenian, R.A. Childs, R.D. Petrasso, V.Yu. Glebov, T.C. Sangster, M. Burke, S. Roberts, The coincidence counting technique for orders of magnitude bachground reduction in data obtained with the magnetic recoil spectrometer at OMEGA and the NIF, *Rev. Sci. Instrum*. 2011, **82**, p. 073502.
[19] F.H. Séguin, N. Sinenian, M.J. Rosenberg, A. Zylstra, M.J.-E. Manuel, H. Sio, C. Waugh, H.G. Rinderknecht, M. Gatu Johnson, J. Frenje, C.K. Li, R. Petrasso, T.C. Sangster, S. Roberts, Advances in compact proton spectrometers for inertial-confinement fusion and plasma nuclear science, *Rev. Sci. Instrum*. 2012, **83**, p. 10D908.
[20] L.F. DeChairo, L.P. Forsley, P. Mosier-Boss, Strained layer ferromagnetism in transition metals and its impact upon low energy nuclear reactions, *J. Condensed Matter Nucl. Sci*. 2015, **17**, p. 6.
[21] X. Zhou, H. Zhao, Z. Fu, J. Qu, M. Zhong, X. Yang, Y. Yi, C. Wang, Nanoporous Ni with high surface area for potential hydrogen storage application, *Nanomater.* 2018, **8**, p. 394.
[22] B. Antolkoviíc, Z. Dolenec, The neuton-induced ^{12}C(n,n')3α reaction at 14.4 MeV in a kinematically complete experiment, *Nuclear Phys. A*, 1975, **237**, p. 235.
[23] S.A.R. Al-Najjar, A. Abdel-Naby, S.A. Durrani, Fast-neutron spectrometry using the triple-α reaction on the CR-39 detector. *Nuclear Tracks*, 1986, **12**, p. 611.
[24] P.A. Mosier-Boss, S. Szpak, F.E. Gordon, L.P.G. Forsley, Triple tracks in CR-39 as the result of Pd-D co-deposition: Evidence of energetic neutrons, *Naturwiss*. 2009, **96**, p. 135.
[25] P.A. Mosier-Boss, J.Y. Dea, L.P.G. Forsley, M.S. Morey, J.R. Tinsley, J.P. Hurley, F.E. Gordon, Comparison of Pd/D co-deposition and DT neutron generated triple tracks observed in CR-39 detectors, *Eur. Phys. J. Appl. Phys*. 2010, **51**, p. 20901.
[26] C. Barras, Neutron tracks revive hopes for cold fusion, *New Scientist* 2009, **201**, p. 10.
[27] P.A. Mosier-Boss, F.E. Gordon, L.P. Forsley, D. Zhou, Detection of high energy particles using CR-39 detectors part 1: Results of microscopic examination, scanning, and LET analysis, *Int. J. Hydrogen Energy* 2017, **42**, p.416.
[28] A.S. Roussetski, A.G. Lipson, E.I. Saunin, F. Tanzella, M. McKubre, Detection of high energy particles using CR-39 detectors part 2: Results of in-depth destructive etching analysis, *Int. J. Hydrogen Energy* 2017, **42**, p.429.
[29] P.A. Mosier-Boss, S. Szpak, F.E. Gordon, L.P.G. Forsley, Characterization of tracks in CR-39 detectors obtained as a result of Pd/D co-deposition, *Eur. Phys. J. Appl. Phys*. 2009, **46**, p. 30901.
[30] D.Z. Zhou, C. Wang, Y.Q. Sun, J.B. Liang, G.W. Zhu, L.P.G. Forsley, P.A. Mosier-Boss, F.E. Gordon, Energetic particles generated in earlier Pd + D nuclear reactions, *J. Condensed Matter Nucl. Sci*. 2015, **15**, p. 33.
[31] M. Macy, Richard Oriani's PACA Protocol, *Infinite Energy* 2015, **123**, p.4.
[32] K.L. Shanahan, Comments on "A new look at low-energy nuclear reaction research," *J. Environ. Monit*. 2010, **12**, p. 1756.
[33] J. Pasley, I.A. Bush, A.P.L. Robinson, P.P. Rajeev, S. Mondal, A.D. Lad. S. Ahmed, V. Narayanan, G.R. Kumar, R.J. Kingham, Generation of shock waves in dense plasmas by high intensity laser pulses, *Nukleonika* 2015, **60**, p. 193.

[34] G.P. Grim, T.N. Archuleta, P.A. Bradley, M.M. Fowler, A.C. Hayes, G. Jungman, A.W. Obst, R.S. Rundberg, D.J. Vieera, Y.Q. Wang, J.B. Wilhelmy, Target debris collection studies for inertial confinement fusion (ICF) experiments, *J. Phys.: Conf. Ser.* 2010, **244**, p. 032046.
[35] M. Karahadian, H.M. Doss. Evidence of particles during electrochemical Pd-D co-deposition, American Physical Society Meeting, Boston, MA, March 2019.
[36] M. Karahadian, A.R. Smith, E. Vahle, H.M. Doss. Investigation of track formation in CR-39 for various hydrated environments, American Physical Society Meeting, Denver, CO, March 2020.
[37] M. Karahadian, A.R. Smith, E. Vahle, Investigation of track formation in CR-39 for various hydrated environments, https://www.researchgate.net/publication/341327123_Investigation_of_Track_Formation_in_CR-39_for_Various_Hydrated_Environments
[38] How to do the exploding pumpkin, https://www.youtube.com/watch?v=epnUKRc8dAo
[39] J. Marwan, M.C.H. McKubre, F.L. Tanzella, P.L. Hagelstein, M.H. Miles, M.R. Swartz. E. Storms, Y. Iwamura, P.A. Mosier-Boss, L.P.G. Forsley, A new look at low-energy nuclear reaction (LENR) research: A response to Shanahan, *J. Environ. Monit.* 2010, **12**, p. 1765.
[40] L. Kowalski, Comments on "The use of CR-39 in Pd/D co-deposition experiments" by P.A. Mosier-Boss, S. Szpak, F.E. Gordon, and L.P.G. Forsley: Interpreting SPAWAR-type dominant pits, *Eur. Phys. J. Appl. Phys.* 2008, **44**, p. 287.
[41] P.A. Mosier-Boss, S. Szpak, F.E. Gordon, and L.P.G. Forsley, Reply to comment on "The use of CR-39 in Pd/D co-deposition experiments": A response to Kowalski, *Eur. Phys. J. Appl. Phys.* 2008, **44**, p. 291.
[42] D. Nikezic, K.N. Yu, Computer program TRACK_TEST for calculating parameters and plotting profiles for pits in nuclear track materials, *Comp. Phys. Commun.* 2006, **174**, p. 160
[43] D. Nikezic, K.N. Yu, Three-dimensional analytical determination of the track parameters: over-etched tracks, *Radiat. Meas.* 2003, **37**, p. 39.
[44] 39. L. Kowalski, Comments on codeposition electrolysis results, *J. Condensed Matter Nucl. Sci.*, 2010, 3, p. 1.
[45] M.E. Little, S.R. Little, "Extraordinary evidence" replication effort, *J. Sci. Explor.* 2009, **2**3, p. 411.
[46] U. Mastromatteo and R. Aina, 'Investigation of Anomalous Densities of High Energy Alpha Particles Tracks in CR-39 Detectors During Electrolysis of Heavy Water on Palladium Cathodes,' in the *15th International Conference on Condensed Matter Nuclear Science* (Rome, Italy, 2010).
[47] P.A. Mosier-Boss, S. Szpak, F.E. Gordon, and L.P.G. Forsley, Comments on co-deposition electrolysis results: A response to Kowalaski' *J. Condensed Matter Nucl. Sci.*, 2010, **3**, p.4.
[48] S.M. Bennington, R.S.Sokhi, P.R.Stonadge, D.K.Ross, M.J.Benham,T.D.Beynon, P. Whithey, I.R. Harris, J.P.G. Farr, A search for the emission of x-rays from electrolytically charged palladium-deuterium, *Electrochim. Acta* 1989, **3**4, p.1323.
[49] M.R. Deakin, J.D. Fox, K.W. Kemper, E.G. Myers, W.N. Shelton, J.G. Skofronick, Search for cold fusion using X-ray detection, *Phys. Rev.* C 1989 **4**0, p. R1851.
[50] L.P. Forsley, P.S. Mosier-Boss, P.J. McDaniel, F.E. Gordon, Charged particle detection in the Pd/D system: CR-39 SSNTD vs. real-time measurement of charged particle stimulated Pd K shell X-rays, *Electrochim. Acta* 2013, **8**8, p.373
[51] M. El Ghazaly and N. M. Hassan, Characterization of CR-39 detector at high alpha-particle fluence, *Nuclear Engineering and Technology* 2018, **50**, p. 432. https://doi.org/10.1016/j.net.2017.11.01
[52] S. Jiang, F. Wang, Y. Ding, S. Liu, J. Yang, S. Li., T. Huang, Z. Cao, Z. Yang, X. Hu, W. Miao, J. Zhang, Z. Wang, G. Yang, R. Yi, Q. Tang, L. Kuang, Z. Li, D. Yang and B. Zhang, Experimental Progress of Inertial Confinement Fusion Based on ShenGuang III Laser Facility in China, *Nuclear Fusion*, 2019, **59,** 032006 p. 11
[53] P.A. Mosier-Boss, L.P.G. Forsley, P.J. McDaniel, The use of CR-39 detectors in LENR experiments,*J. Condensed Matter Nucl. Sci.* 2014, **14**, p. 29.
[54] A.G. Lipson, A.S. Roussetski, E.I. Saunin, F. Tanzella, B. Earle, M. McKubre, Analysis of the CR-39 detectors from SRI's SPAWAR/Galileo type electrolysis experiments #7 and #5. Signature of possible neutron emission, in *Proceedings of* 8^{th} *International Workshop on Anomalies in Hydrogen/Deuterium Loaded Metals* ed. J. Rothwell and P. Mobberley (The International Society for Condensed Matter Nuclear Science, 2008).
[55] S.B. Krivit, J. Marwan, A new look at low-energy nuclear reaction research, *J. Environ. Monit.* 2009, **11**, p. 1731.

[56] S. Gaillard, J. Fuchs, N. Renard-Le Galloudec, T.E. Cowan, Study of saturation of CR39 nuclear track detectors at high ion fluence and of associated artifact patterns, *Rev. Sci. Instrum*. 2007, **78**, p. 013304.